submitted to *Geophys. J. Int.*

Shear-wave splitting beneath Fennoscandia - Evidence for dipping structures and laterally varying multi-layer anisotropy

Manuscript accepted by Geophysical Journal International
The final publication is available at https://academic.oup.com/gji
via https://doi.org/10.1093/gji/ggaa388

Michael Grund, Joachim R. R. Ritter

Karlsruhe Institute of Technology (KIT), Geophysical Institute, Hertzstr. 16, 76187 *Karlsruhe, Germany.*

Email: michael.grund@kit.edu

SUMMARY

The geodynamic evolution of Fennoscandia in northern Europe (Finland, Sweden, and Norway) is coined by ca. 3 Ga history of tectonic processes including continental growth in its central and eastern parts and Neogene uplift processes of the Scandinavian mountains (Scandes) located along its western edge. Many details are still under debate and we contribute with new findings from studying deep-seated seismic anisotropy. Using teleseismic waveforms of more than 260 recording stations (long-running permanent networks, previous temporary experiments and newly installed temporary stations) in the framework of the ScanArray experiment, we present the most comprehensive study to date on seismic anisotropy across Fennoscandia. The results are based on single and multi-event shear-wave splitting analysis of core refracted shear waves (*SKS*, *SKKS*, *PKS*, *sSKS*). The splitting measurements indicate partly complex, laterally varying multi-layer anisotropy for individual areas. Consistent measurements at permanent and temporary recording stations over several years and for seismic events of specific source regions allow us to robustly constrain dipping anisotropic structures by adding systematic forward modeling. Although the data coverage is partly limited to only few source regions, our findings support concepts of continental growth due to individual episodes of (paleo-) subduction, each affecting a plunging of the anisotropic fast axis direction due to collisional deformation. Along the northern Scandes the fast axis direction (ϕ) is parallel to the mountain range (NE-SW), whereas a NNW-SSE trend dominates across the southern Scandes. In the south, across the Sorgenfrei-Tornquist Zone, a NW-SE trend of ϕ dominates which is parallel to this suture zone. The Oslo Graben is characterised by a NNE-SSW trend of ϕ. In northern Norway and Sweden (mainly Paleoproterozoic lithosphere), a dipping anisotropy with ϕ towards NE prevails. This stands in contrast to the Archean domain in the NE of our study region where ϕ is consistently oriented NNE-SSW. In the Finnish part of the Svecofennian domain, a complex two-layer anisotropy pattern is found which may be due to lateral variations around the seismic stations and which requires a higher data density than ours for a unique model building. Based on these findings our study demonstrates the importance of long recording periods (in the best case > 10 years) to obtain a sufficient data coverage at seismic stations, especially to perform meaningful structural modeling based on shear-wave splitting observations.

Key words: Seismic anisotropy; Dynamics of lithosphere and mantle; Time-series analysis

1 INTRODUCTION

The present-day shape of the Fennoscandian peninsula was formed during several collision and rifting events within the last 3 Ga, each affecting comprehensive reworkings of the lithosphere and the surface (Fig. 1). A major tectonic episode, the Caledonian orogeny, was initiated around 500 Ma ago by the closing of the Iapetus Ocean. In the following, the Caledonian mountain belt was formed due to the collision of the paleo-continents Laurentia and Baltica/Avalonia 430-410 Ma ago (e.g. McKerrow et al., 2000; Roberts, 2003; Torsvik & Cocks, 2005). Furthermore, it is well accepted that Baltica was partially subducted towards west beneath Laurentia during the orogenesis (e.g. Krogh, 1977; Roberts, 2003; Gee et al., 2008). Finally, the opening of the North Atlantic Ocean around 55 Ma ago separated the Caledonides whose fragments at present are located along the western rim of Fennoscandia as well as in North America, Greenland and Scotland. Remnants of the mostly eroded Caledonides form part of the Scandinavian Mountains (Scandes) with large nappes covering the western edge of Baltica (Fig. 1, e.g. Gaál, 1986; Gaál & Gorbatschev, 1987). The Scandes are located at a passive continental margin which spans along the western rim of Fennoscandia, far away from active plate tectonics. However, the topography of the mountain chain with elevations of up to 2000-2500 m (especially in the south) is still higher than expected for such an old orogen (e.g. Nielsen et al., 2009) and therefore processes within the Earth's mantle most likely play an important role in explaining the current shape of the Scandes (for a review see e.g. Maupin et al., 2013). Prior to the Caledonian orogeny, the Baltic Shield with its Archean, Svecofennian and Sveconorwegian provinces (Fig. 1) grew during several collisional phases including the accretion of individual micro-plates and oceanic arcs (e.g. Gaál & Gorbatschev, 1987; Lahtinen et al., 2005; Korja et al., 2006). Dipping reflectors observed in reflection seismic profiles were partly interpreted as relicts of paleo-subduction (e.g. BABEL Working Group, 1990; Balling, 2000, see "sawtooth" lines in Fig. 1). In the southwest the Sorgenfrei-Tornquist Zone (STZ) separates the Precambrian Baltic Shield from the Phanerozoic terranes of Central Europe (e.g. Berthelsen, 1992; Zielhuis & Nolet, 1994). The generally NW-SE oriented STZ represents the northwestern extension of the Trans-European Suture Zone (TESZ) that resulted from the collision of Baltica with Avalonia around 450 Ma ago after the closing of the Tornquist Sea (e.g. Pharaoh, 1999; Torsvik & Rehnström, 2003, see also Fig. 1 right). Each of these events caused a characteristic signature of deformation due to compressional or extensional regimes.

Seismic anisotropy is one of the key tools to investigate dynamic-driven processes in the Earth's interior. In this context the anisotropic signatures can provide valuable information about current and past deformation processes or mantle flow in the Earth's crust as well as the upper and lowermost mantle (e.g. Babuška & Cara, 1991; Savage, 1999; Fouch & Rondenay, 2006; Long & Silver, 2009).

A shear-wave that propagates through a volume of anisotropic material is split into two orthogonally polarized shear-waves that travel with different speeds, polarized in the fast and slow directions of the medium (Silver & Chan, 1991; Savage, 1999; Long & Silver, 2009). The azimuthal orientation of the fast polarization axis direction (ϕ) and the delay time (δt), accumulated between the two split waves, are known as the splitting parameters. They can be measured at a seismic recording station at the Earth's surface. Commonly core-refracted shear-waves like *SKS*, *SKKS* or *PKS* are used to constrain the anisotropy. Their radial polarization after the *P*-to-*S* conversion at the core-mantle boundary (CMB) ensures that the splitting, if observed, is generated on the receiver side of the travel path. Furthermore, the initial polarization of core-refracted phases coincides with the event backazimuth (BAZ) and is therefore a known quantity (e.g. Savage, 1999). Due to their nearly vertical propagation paths, splitting measurements of these phases made at dense recording networks provide very good lateral resolution. In contrast, the depth location of the anisotropic medium between CMB and surface cannot be determined from individual splitting observations alone. Comparisons with estimates from surface wave data (e.g. Zhu & Tromp, 2013; Yuan & Beghein, 2014) as well as discrepancies between phases measured in the same seismogram (e.g. *SKS* and *SKKS*), however, can give us a hint toward the depth range of the anisotropy (e.g. Hall et al., 2004; Lynner & Long, 2012; Grund & Ritter, 2019). Additionally, more recent work demonstrates that it is also possible to determine some depth constraints based on finite frequency splitting analysis (Mondal & Long, 2019, 2020).

Although splitting measurements are often associated with only a single, horizontal layer of anisotropy, variations of ϕ and δt with respect to the backazimuth and incidence angle indicate more complex structures (e.g. Silver & Savage, 1994; Hartog & Schwartz, 2000; Marson-Pidgeon & Savage, 2004). Depending on the structural complexity, characteristic patterns of measured apparent splitting parameters allow to identify the underlying anisotropy. Seismic anisotropy studies can therefore be used to reveal past (and current) episodes of deformation within the different provinces of Fennoscandia.

Here we use the massive seismological data set acquired within the framework of the ScanArray initiative (Fig. 2a) to study seismic anisotropy of the lithosphere-asthenosphere system beneath Fennoscandia. The aims are to find anisotropy structures which can be related to past deformation processes as well as present asthenospheric flow pattern. The station coverage allows us to explore areas without previous splitting observations as well as use long-term observations at permanent stations which were not fully studied up to now. From the long-term recordings we expect splitting observations from different azimuths to test existing simple models based on few observations and to derive, if necessary, more complex models including lateral variations and inclined layer geometries. In this way the above described geodynamic setting will be validated, improved, and refined.

We conducted a systematic shear-wave splitting analysis at 266 seismic broadband stations located across whole Fennoscandia and surrounding countries. For permanent stations, that were previously analyzed, now additional 10 more years of continuous data are available in some cases. With 6467 uniformly processed single-event shear-wave splitting measurements (1772 splits and 4695 nulls) and 154 multi-event measurements (stacked splitting results of poor quality) we are able to constrain so far poorly or completely unresolved features related to tectonic deformation in this area. Furthermore, some blank spots along the northern Scandes are explored for the first time. At several stations (mostly long-running permanent ones) we can clearly model the observations with a dipping anisotropic fabric (only based on shear-wave splitting measurements). Strong indicators for laterally varying anisotropy around the single stations are also found for individual areas. Splitting measurements at some of the stations also show characteristics of a two-layer system. However, for these we cannot fully resolve a unique model that can explain both, the fast axis orientations and delay times simultaneously. Together with new constraints from other methodologies based on ScanArray data, the observations will allow to increase our knowledge regarding the tectonic evolution of Fennoscandia.

2 PREVIOUS ANISOTROPY STUDIES

The anisotropic structure beneath Fennoscandia and neighboring terranes, including the most western parts of the East European Craton (EEC) and the STZ suture zone, were repeatedly a subject of research in the last two decades. In this context shear-wave splitting studies were mostly conducted in specific tectonically and geologically interesting areas with data of temporary seismological experiments. **Fig. S8** (see Supporting Information) gives an overview of past shear-wave splitting studies in Scandinavia including the projects SVEKALAPKO in southern and central Svecofennia/Finland (Vecsey et al., 2007), LAPNET in northern Finland (Vinnik et al., 2014), MAGNUS, SCANLIPS, SCANLIPS2 (Roy & Ritter, 2013) and TOR (Wylegalla et al., 1999; Plomerová et al., 2002a) as well as measurements at seismic stations of the Swedish National Seismic Network (SNSN, Eken et al., 2010) and single measurements from some other stations (Vinnik et al., 1992; Wüstefeld et al., 2010) of the early Global Digital Seismograph Network (GDSN). Besides shear-wave splitting, partly also *P*-wave analysis and surface wave data were used to constrain the anisotropic pattern (e.g. Plomerová et al., 2002b; Pedersen et al., 2006). For larger scales, the measured shear-wave splitting parameters can be compared with seismic anisotropy models that cover most parts of Europe (e.g. Zhu & Tromp, 2013; Zhu et al., 2015). Partly contradictory explanations were found for the observed anisotropy, ranging from the mostly preferred theory of fossil frozen-in anisotropy, represented by spatially varying signatures across the different accreted terranes of Fennoscandia (Plomerová et al., 2001; Plomerová et al., 2002a; Plomerová et al., 2006; Vecsey et al., 2007; Eken et al., 2010; Plomerová et al., 2011; Munzarová et al., 2018), to multi-layered anisotropy with contributions also from asthenospheric mantle flow in northern Finland (Vinnik et al., 2014). For southern Norway complex and deeply located anisotropy was inferred (Roy & Ritter, 2013) based on large delay times and varying fast axis orientations. Measurements at temporary stations along or close to the STZ mostly offered fast axis orientations parallel to the strike of the suture (Wylegalla et al., 1999) which may be related to the collisional processes between Avalonia and Baltica.

3 DATA AND METHODS

3.1 Seismic networks and data coverage

We analyzed data of in total 266 seismic broadband recording stations for shear-wave splitting (Fig. 2a). Most stations were part of the international ScanArray initiative which includes the temporary deployments ScanArray Core (Thybo et al., 2012; Grund et al., 2017a), Neonor2 (Gradmann et al., 2014) and SCANLIPS3D (England et al., 2015). The inter-station distance was typically less than 50 km. Besides these three newly recorded data sets, we re-examined some stations of the temporary MAGNUS project (Weidle et al., 2010) to ensure a consistent data processing for later comparison. At MAGNUS stations shear-wave splitting was previously studied by Roy & Ritter (2013). Furthermore, high-quality data of several permanent networks in Fennoscandia and surrounding countries were analyzed (136 stations). At permanent stations, that were also studied in the past, the analysis was continued with more recent recordings. Data coverage ranges from only a few months (some temporary deployments) up to more than 15 years at permanent stations, especially in Finland and Norway. For most stations of ScanArray Core the recording times ranged between two and four years. From the Swedish National Seismic Network (SNSN, 1904) a limited subset of four years of restricted data was examined (2012-2016), however, some open stations available from ORFEUS were analyzed for longer periods. This represents a continuation of the work done by Eken et al. (2010) for the period 2002-2008, however, in the meanwhile several new recording stations were installed within the SNSN network.

Based on the Global CMT catalog (Dziewoński et al., 1981; Ekström et al., 2012) we selected around 3000 teleseismic earthquakes with moment magnitude M_{w} 5.5 or greater at epicentral distances between 80° and 140°. All events have hypocenter depths $>$ 20 km and occurred between March 1998 and October 2017. After applying strict quality criteria (see below), the recordings of 541 events allowed to make at least one reliable splitting measurement at any of the studied seismic stations (Fig. 2b). In Fennoscandia the data coverage in general is dominated by events located between Indonesia and the Eastern Pacific region as well as South and Central America. Depending on the individual recording periods of the stations also waveforms are available of a few events from the South Sandwich Island area as well as one event (with in total four reliable measurements) from beneath Big Island (Hawai'i) in 2006. For backazimuthal directions in between, no data for the selected criteria are available which is mainly caused by the uneven distribution of global seismicity preferentially located along deep subduction zone systems and plate boundaries. The largest backazimuthal gap ranges from around 110° to 200° (Fig. 2b).

3.2 Single- and multi-event splitting measurements

Prior to the splitting analysis we applied a zero-phase butterworth band-pass filter (5 s - 15 s) to remove noise and frequencies of no interest from the waveforms. Partly the corner periods were slightly adjusted to improve the signal-to-noise ratio (SNR) and improve the waveform clarity as done in previous work (e.g. Eakin et al., 2016; Grund, 2017; Grund & Ritter, 2019). Measurements for which a clear discrepancy in splitting intensity (Chevrot, 2000; Deng et al., 2017) between *SKS* and *SKKS* for the same source-receiver configuration was observed were removed from the data set since they are assumed to be contaminated by contributions from anisotropy in the lowermost mantle beneath Siberia and the Atlantic (Grund & Ritter, 2019).

Splitting measurements of single-phase arrivals (*SKS*, *SKKS*, *PKS*, *sSKS*) were conducted with the SplitLab toolbox (Wüstefeld et al., 2008). We simultaneously applied two different analysis approaches, namely the rotation-correlation method (hereinafter RC, e.g. Bowman & Ando, 1987) and the energy minimization method (SC, Silver & Chan, 1991) to determine the two splitting parameters, fast direction ϕ and delay time δt. Possible sensor misorientations were corrected by comparing the SC and RC outputs (e.g. Tian et al., 2011; Grund & Ritter, 2019; Grund, 2019b). Determined misorientations for ScanArray stations can be found in Grund et al. (2017a) and **Table S1** (Supporting Information). For the analyzed MAGNUS stations we considered the previously identified sensor misalignments listed in Wawerzinek (2012).

Only measurements for which both methods agreed within their error bounds (95% confidence region, corresponding to 2σ), for which the deviations of the initial polarization from the backazimuth were less than $\pm$ 10° and which have SNRs larger than 5 were considered (e.g. Long & Silver, 2009). Depending on the errors, we ranked measurements of clearly split phases as *good* (95% confidence region of up to $\pm$ 15° in ϕ and $\pm$ 0.2 s in δt) or *fair* ($\pm$ 25° in ϕ and $\pm$ 0.5 s in δt). A waveform example is shown in Fig. 3. Phase arrivals with an SNR of greater than 5 on the radial component, nearly no signal (except the background noise) on the transverse component, and (nearly) linear particle motion before the correction for splitting are indicative for the absence of splitting. According to the split phases we classified these so-called null measurements as *good* or *fair* (Wüstefeld & Bokelmann, 2007), depending on the noise level on the transverse component and the linearity of the particle motion (a corresponding waveform example can be found in **Fig. S9**, Supporting Information). The uncertainties were calculated using the corrected and updated formulation of Walsh et al. (2013) as implemented in the SplitLab plugin StackSplit (Grund, 2017). StackSplit was also used to calculate in total 154 multi-event splitting results from low-quality measurements at several stations using the energy surface stacking technique (WS, Wolfe & Silver, 1998, see Table **S2**). However, due to partly strong directional variations of the splitting parameters, we only stacked measurements (if enough were available) within 5° bins with respect to backazimuth and epicentral distance (detailed information can be found in the Supporting Information). By this it was possible to increase the number of measurements at some stations. Although it was inferred that simple averaging gives similar results if ϕ and δt are invariant with respect to the backazimuth (Kong et al., 2015), the WS method further allows us to directly calculate formal errors from the stacking procedure. Exemplary diagnostic plots of multi-event measurements can be found in **Fig. S1** of the Supporting Information as well. In the following only the SC (single splits) and WS results are shown.

4 SHEAR-WAVE SPLITTING RESULTS

4.1 General trends and geographical variations

From the systematic shear-wave splitting analysis in total we received 1772 measurements of clearly split phases and almost two and a half times more null observations (4695). As mentioned before, discrepant pairs are not included (Grund & Ritter, 2019) in this data set. The individual splitting measurements are summarized in Fig. 4. The average fast polarization direction has roughly a NE-SW orientation for this data set. However, in a histogram representation the data reveals a clear trimodal distribution (Fig 5) for the fast axis ϕ with the three peaks at around $-75°$ (WNW-ESE), 22° (NNE-SSW) and 75° (ENE-WSW). In contrast, the delay times δt are almost evenly distributed around the average value of 1.04 s with a slight trend to larger values (Fig 5). This is consistent with the globally observed average delay times of around 1 s for continental regions (e.g. Silver, 1996; Fouch & Rondenay, 2006).

If only results of stations in specific geographic areas are considered, clear lateral variations become obvious (especially for ϕ). For instance, in central and northern Norway/Sweden the dominant directions of ϕ with 55°-75° are close to the strike of the Scandinavian mountains. The average ϕ for stations located in the area with the highest topography of the Scandes in southern Norway, however, shows a trend of around $-10°$. In contrast, southern Finland seems to be a more complex area with a clear bimodal distribution for ϕ (Fig 5). The delay times for all regions show only slight variations and contribute similarly to the overall (unimodal) trend of the whole data set presented in the top row of Fig 5.

At several recording stations, both temporary as well as long-running permanent ones, only nulls are observed for all phase arrivals (Fig. 4). However, this does not necessarily mean that the structure beneath the corresponding station is purely isotropic. Nulls can also be indicative for scenarios in which the initial polarization of the shear-wave is parallel to the fast axis ϕ of the anisotropic medium (or perpendicular to it) or that the splitting is cancelled out due to multiple layers of anisotropy (e.g. Barruol & Hoffmann, 1999). Furthermore, it could be possible that the results obtained from waveforms with some energy on the transverse component did not meet the appropriate quality criteria we applied during the pre-processing. However, it is not possible to clearly identify regions with only null observations. It seems that most nulls are distributed across central and northern Sweden and Norway (Fig. 4).

4.2 Stereoplot representation

Besides the clear lateral variations of ϕ between different areas in the study region (Fig 5), variations at several stations themselves can be observed in Fig. 4. These can be most easily visualized by so-called stereoplots in which the splitting parameters of each individual station are plotted as a function of backazimuth (clockwise direction from north) and incidence angle (radial axis). An overview of the direction-dependencies (based on different event source regions) in map-view is contained in the Supporting Information (**Figs. S10** to **S15**).

Based on their stereoplot patterns we divided the splitting characteristics of the 266 analyzed stations into four different classes:

(i) simple (no or only negligible backazimuthal variations), **109** stations
(ii) complex (strong variations of ϕ and/or δt with backazimuth), **53** stations
(iii) null (dominated by nulls), **63** stations
(iv) poor (less than five *good*/*fair* split or null measurements are available), **41** stations.

In Fig. 6 we present exemplary stereoplots of six different recording stations located across the study region (highlighted by blue circles in Fig. 2) that were classified into the first three categories. Stereoplots for all analyzed stations (including stations ranked *poor*) can be found in the Supporting Information. The top row shows two examples of the first class with relatively simple splitting characteristics and negligible azimuthal variability. At permanent station HAMF we observe a bunch of consistent splits (similar ϕ and δt) for phase arrivals in the northeastern quadrant (backazimuths of 0° to 90°). Although no splits were measured in the other quadrants, the locations of nulls along the orientation of ϕ and nearly perpendicular to it, allow to characterize the anisotropy beneath the station by a single horizontal layer (e.g. Silver & Savage, 1994).

A similar pattern (but with different ϕ and δt) was observed at temporary station NWG28 (MAGNUS project) that was installed in southern Norway. However, one further split with consistent ϕ and δt was measured in the southwestern quadrant. In contrast, nulls were only found for the direction perpendicular to the dominant orientation of ϕ in the northeastern and southwestern quadrants.

The middle row of Fig. 6 displays splitting results for two stations at which we observe complex splitting patterns with mostly significant azimuthal variability. While the orientations of ϕ at permanent station VAF can be clearly divided into three backazimuthal domains, each with an individual dominant direction ($\sim 70°$: bluish color, $\sim 5°$: greenish and $\sim -60°$: orange), the corresponding delay times are nearly constant except for the waves from western directions with slightly larger values. In between several nulls are located without a clear first-order trend.

At temporary station SA64 the variation is not as significant as at station VAF, however, the color-coding indicates a slight rotation of ϕ towards $\sim 30°$ for backazimuths around 90°. The delay times show no significant variability. Besides the robust v-shaped pattern formed by the two groups of splits (for details see Supporting Information, **Figs. S3** and **S5**), measured nulls are mostly located between them and in the southwestern quadrant.

The stereoplots shown in the bottom row of Fig. 6 represent two stations at which we did not observe any splitting. This means that for all shear-wave splitting measurements clear nulls were determined independent from the backazimuth. However, as mentioned before, this does not necessarily mean that the sampled structures beneath the station are of isotropic character.

Displaying the different stereoplots in map view allows us to identify areas of similar splitting character and therefore abrupt or smooth lateral inter-station variations. In Fig 7 we highlight our findings for southern Norway, Sweden and northern Denmark (an overview for the area of southern Finland can be found in **Fig. S16** of the Supporting Information). Here we can clearly divide the splitting patterns into two groups. While southern Norway on average is dominated by a fast axis direction of around $0°$ to $-20°$ (teal area), south-east of this group towards southwestern Sweden the orientation of ϕ slightly rotates toward $-60°$ (orange area). In general, this orientation matches quite well with the strike of the STZ. A significant change can be observed for station BSD where the orientation of ϕ is aligned in almost N-S direction. This is very similar to the findings of Wylegalla et al. (1999) and therefore supports the interpretation that the orientation of ϕ is most probably related to the N-S striking segment of the STZ in this area (Fig 7).

The observations at the stations of NORSAR (Fig. 7a) are mostly dominated by null measurements from different directions. Partly consistent splits can only be observed at stations NC204, NBO00, NC303 and NC405. However, for NC204 and NC303 the majority of nulls corresponds to backazimuth directions which are nearly perpendicular to the measured fast axis orientation. Furthermore, the perpendicular-to-backazimuth direction for these nulls is close to the general fast direction of the nearby teal region. This allows us to assume that a simple horizontal layer of anisotropy is responsible for the observed splitting. Moreover, it seems that a robust determination of multi-layer anisotropy scenarios at the long-running NORSAR stations (1998-2017), using only core refracted shear-waves, is quite impossible due to the unfavorable distribution of seismicity and resulting gaps in the backazimuthal data coverage (Fig. 2). The pattern at the long-running permanent station KONO, located southwest of NORSAR at the western rim of the Oslo Graben (Fig 7b), only differs significantly at certain backazimuths in comparison to the surrounding stations. The dominant fast axis orientations vary between $10°$ and $45°$. Nevertheless, these are consistent within narrow backazimuthal ranges and point towards a more complex scenario (see modeling below).

For stations at which no (or only negligible) backazimuthal variations were found (class 1), we calculated station averages for ϕ and δt using the WS method as implemented in StackSplit (see Supporting Information). By this we get for each of the corresponding stations a single set of splitting parameters which characterize a single horizontal layer of anisotropy. However, due to backazimuthal gaps in the data, we cannot fully rule out that a more complex anisotropic structure is located beneath the stations. For stations belonging to the second group ("complex") we performed detailed forward modeling. Stations sorted into the last class (*poor*) were discarded for further analysis since the data availability does not allow an adequate modeling of anisotropic structure. Null stations were also not modeled but integrated in the final discussion and interpretation.

5 MODELING OF COMPLEX SPLITTING PATTERNS

In order to constrain the underlying anisotropy system for stations sorted into class 2 (complex), we performed systematic forward modeling using the MATLAB Seismic Anisotropy Toolkit (MSAT, Walker & Wookey, 2012). For this purpose we first pre-computed synthetic splitting parameters for shear-waves of 8 s dominant period (typical for the recorded *SKS*, *SKKS*, *PKS* and *sSKS* phases) that propagate through models consisting of two anisotropic layers or one layer with a dipping symmetry axis (technical details can be found in the Supporting Information). Two-layer models, for instance, may represent a continental lithospheric layer dominated by fossil frozen-in seismic anisotropy atop an asthenospheric layer that reflects anisotropy induced by current horizontal mantle flow. Inclined structures related to relicts of paleo-subduction may be characterized by models with a dipping symmetry axis. Although this modeling approach is based on ray theory and generally ignores important seismic wave properties like finite-frequency effects, the results provide valuable information about potential first-order anisotropy characteristics beneath a seismic recording station (e.g. Walker & Wookey, 2012; Aragon et al., 2017).

In most cases the model-fit is based on a limited backazimuthal range which preferentially contains a large number of observations. This allows us to constrain a model for a specific backazimuthal region, even if the splitting pattern indicates additional lateral variations. To find for each station a model that best fits the data the minimum root-mean-square error (RMSE) between the predicted splitting parameters and the measured values was determined using:

$$\mathrm{RMSE} = \sqrt{\frac{1}{i}(x_1^2 + x_2^2 + ... + x_i^2)} \tag{1}$$

with i representing the number of measured data points and x the difference between model curve and each individual data point. Following Liddell et al. (2017) the misfits for ϕ (RMSE$_\phi$) and δt (RMSE$_{\delta t}$) were normalized separately by the maximum observed value (90° for ϕ and 4 s for δt) to ensure that both RMSE values equally contribute to the overall misfit (RMSE$_{tot}$). Thus, RMSE$_{tot}$ is a dimensionless quantity.

In Fig. 8 we show exemplary modeling results for three stations (highlighted by orange circles in Fig. 2) at which a dipping structure represents the most plausible model-fit (lowest RMSE) based on an observational backazimuthal limitation indicated as white sector in the stereoplots. The full range of tested models can be found in the Supporting Information. Although only limited data contributes to the model, the v-shaped pattern indicative for a dip of the anisotropy fast axis as well as the predicted locations of nulls, are confidently reproduced by the best-fit parameter set which in these three cases corresponds to relatively steeply dipping layers with dip directions towards north-east (Fig. 8, bottom row). Furthermore, the layer dip as well as the down-dip directions are quite robustly determined at all three stations (Fig. 8, middle row). None of the tested two-layer models is able to explain the observed splitting parameters at these stations in a similar way. Further details about the modeling of other stations and possible non-uniquenesses are discussed by Grund (2019b).

In Fig. 9 we summarize our modeling results for all recording stations together with the major tectonic units of Fennoscandia. Modeling details for each station can be found in Table **S3** in the Supporting information. Besides areas in which simple splitting pattern allowed to calculate station averages using the method of Wolfe & Silver (1998), for some regions the observed splitting can be robustly modeled with a dipping symmetry axis, similar to the examples presented in Fig. 8 for stations OUL, TRO and RATU. Stations at which a complex splitting pattern did not allow to quantify a unique model are highlighted as red dots. Here, partly two-layer characteristics are observed which, however, cannot be explained simultaneously by delay time and fast axis orientation (see following sections).

6 DISCUSSION AND INTERPRETATION

While structural models with two stacked horizontal anisotropic layers are often used to explain variations of the splitting parameters with backazimuth (e.g. Silver & Savage, 1994; Levin et al., 1999; Currie et al., 2004; Yang et al., 2014), the detection of systems with a dipping symmetry axis from shear-wave splitting measurements alone is limited to only few studies (e.g. Hartog & Schwartz, 2000; Hicks et al., 2012; Liddell et al., 2017). There are many more cases in which a dip of the symmetry axis was inferred by the joint inversion of different body wave types, especially for some areas of the Fennoscandian Peninsula (e.g. Babuška et al., 1993; Plomerová et al., 2006; Vecsey et al., 2007).

6.1 Can the splitting patterns be associated with tectonic units and events?

Discussing the modeling results in the context of the tectonic and geological evolution of Fennoscandia (Fig. 9) allows us to associate some of the splitting characteristics with past deformation events.

6.1.1 Southern Norway, northern Denmark and western Sweden (55°N - 62°N)

The simple pattern for most stations located in southern Norway, northern Denmark and western Sweden allowed us to calculate station averages for ϕ and δt, although the data coverage is mostly limited to two quadrants in stereoplot view (Fig. 7) and, therefore, more complex models cannot fully be ruled out. As indicated before, the orientation of ϕ smoothly rotates from around $0°$ to $-20°$ in southern Norway to a $-60°$ orientation further east (Sveconorwegian domain, orange) which is parallel to the dominant strike of the STZ. This suture zone is related to the collision of Avalonia and Baltica which caused large-scale deformation in the crust and mantle (e.g. Torsvik & Rehnström, 2003). The estimated width of the STZ is still under debate. Kind et al. (1997) observe a sharp (~ 5 km) change in phase conversions of teleseismic waves at the Moho across the STZ. Teleseismic travel time residuals also indicate a rather sharp lithospheric change (Pedersen et al., 1999). This observation is in contrast to active source experiments which indicate a wider transition zone (Eugeno-S Working Group, 1988). A summary of the width of this deformation zone can be found in Gregersen et al. (2002) who also favour a sharp transition. Although the seismic properties constrained by tomographic images in general offer differences between the Proterozoic Europe and the Precambrian Baltic Shield (e.g. Zielhuis & Nolet, 1994), more recent regional studies (based on *P*- and *S*-waves) consistently show a sharp contrast for seismic velocities that separates southern Norway and northern Denmark from shield areas east of the Oslo Graben (Medhus et al., 2009, 2012; Wawerzinek et al., 2013). This transition zone roughly coincides with the observed rotation of ϕ and stretches nearly in N-S direction across the Oslo Graben area. The anisotropic signatures at stations located on both sides of the STZ in Denmark and southwestern Sweden, however, do not differ significantly. The delay times observed for southern Norway (averages of 0.7 s to 1 s) are generally smaller than the previously reported values by Roy & Ritter (2013). However, for some stations δt is up to 1.5 s on average (Fig. 9). Since these values significantly exceed the typically observed magnitude for crustal anisotropy of 0.2 s to 0.3 s (Crampin & Booth, 1985; Barruol & Mainprice, 1993), a strong contribution from deeper structures such as the mantle lithosphere is necessary to explain the relatively large delay times. This is supported by a similar pattern (ϕ and δt) that was previously observed based on data of the temporary TOR experiment and that was associated with vertically coherent deformation of the lithosphere (Wylegalla et al., 1999). With our increased data coverage, being available now, this spatial correlation becomes more obvious.

While generally similar orientations for ϕ were observed in the past at station KONO (Vinnik et al., 1992; Wylegalla et al., 1999; Roy & Ritter, 2013), the characteristic v-shaped pattern in the stereoplot (Fig. 7b) for the northeastern quadrant has not been documented so far. The formation of the Oslo Graben was accompanied by several epsiodes of compressional and extensional deformation related to changing stress fields (Heeremans et al., 1996). In the case of vertically coherent deformation of the crust and upper mantle caused by rifting, ϕ would align parallel to the dominant extension direction of the graben in E-W direction (e.g. Silver, 1996). A compressional stress regime with the maximum horizontal stress component σ_1 aligned in nearly NW-SE direction would instead affect anisotropy due to mantle minerals with a lattice-preferred orientation (LPO) of ϕ normal to the principal stress component in NNE-SSW direction. This correlates well with the NNE down-dip direction of our best-fit dipping layer model scenario for station KONO (Fig. 10). Therefore, the ϕ orientation (strike of the presumed dipping structure beneath KONO) may be related to the Caledonian orogeny whose assumed suture is nearly parallel to the modeled fast axis orientation and which is assumed to have caused a significant tectonic imprint in the Oslo Graben area (Heeremans et al., 1996). An alternative explanation for a graben-parallel orientation of ϕ are dykes related to massive fissure volcanoes which erupted parallel to the strike of the rift. This Permo-Carboniferous large-scale dyke-related magmatisms, with preferred N-S alignment, is summarized e.g. in Larsen et al. (2008). The dip of ϕ may be explained by either inclined dyke structures or subsequent tectonic processes. The splitting observations in the southwestern quadrant (Fig. 10), not included in the modeling for a dipping layer, most likely reflect anisotropy related to deformation caused by the collision of Avalonia and Baltica (similar ϕ as the stations in southern Norway) and sampled by waves arriving from backazimuths of 230° to 270°. A possible two-layer scenario at KONO also considers a combination of deformation processes related to the Avalonia-Baltica collision and an imprint due to the Oslo Graben complex. The fast axis orientation in the upper layer (ϕ_{upp} = -30°) of the best-fit model displayed in Fig. 10 corresponds to the direction of the surrounding stations in southern Norway, while for the lower layer (ϕ_{low} = 50°) the orientation is parallel to the strike of the graben. Although this two-layer model seems to be an alternative explanation for the observations, various other models with partly distinct differences for ϕ_{upp} , ϕ_{low}, δt_{upp} and δt_{low} can explain the data in a similar way (Grund, 2019b) and therefore KONO is highlighted as complex in Fig. 9.

For stations located east and west of the Sveconorwegian deformation zone (SNDF) the orientations of ϕ abruptly change from a nearly N-S direction on the Sveconorwegian domain (Fig. 9, orange) to an E-W alignment on the Transscandinavian Igneous Belt (TIB, brown) and the Svecofennian domain (pink). The western stations fit into the overall picture by representing a smooth rotation towards the STZ-parallel ϕ direction observed at stations further south. This pattern has not been documented in such detail before since previously analyzed stations of the SNSN (Eken et al., 2010) were located only east of the deformation zone. The results of Eken et al. (2010) for the eastern part based on joint inversions of shear-wave splitting measurements and *P*-wave residuals, however, are generally consistent with our findings based on more recent data. Furthermore, few observations of variations across the SNDF from a short-running temporary deployment were limited to a relatively small area at around 60°N (Plomerová et al., 2001). Such abrupt changes of ϕ within short distances are strong indicators for fossil frozen-in anisotropy (e.g. Chevrot et al., 2004) that was imprinted into individual mantle lithosphere fragments before their accretion onto the Baltic Shield (e.g. Plomerová et al., 2001; Plomerová et al., 2002a; Eken et al., 2010). At this point it has to be mentioned that observed *P*-wave residuals may also be attributed to isotropic velocity heterogeneities and, therefore, it is difficult to distinguish them from likely anisotropic contributions (Plomerová et al., 2006).

6.1.2 Central Norway and Sweden (62°N - 65°N)

A more complex picture appears for the Svecofennian domain in eastern Sweden up to around 65°N latitude. Although it was possible to calculate simple station averages with dominantly E-W orientations for ϕ and 0.7 s to 1.3 s for δt at several stations assuming one anisotropic layer with horizontal symmetry axis, observations of some sites in between were best fitted by a dipping layer geometry (Fig. 9). As already pointed out by Eken et al. (2010) the varying splitting patterns (different ϕ and dip angles) south of 61° N indicate complex anisotropy within short lengthscales.

West of the Svecofennian domain atop the Caledonian nappes the recording stations are dominantly characterized by nulls. However, at this point it has to be mentioned that for some of these stations the azimuthal data coverage was worse compared to other stations across the study region. Therefore, this pattern may also reflect poor sampling of (potentially) anisotropic structure and does not necessarily mean that an (apparently) isotropic rock volume is located beneath this area. Alternatively, the presence of two anisotropic layers with orthogonal symmetry axes but similar strengths (e.g. Silver & Savage, 1994) or vertical mantle flow as suggested for other regions like the eastern North American margin (e.g. Lynner & Bodmer, 2017) would result in apparent null observations. Although from seismic tomography a low velocity zone in the upper mantle beneath southern Norway was inferred (e.g. Wawerzinek et al., 2013; Rickers et al., 2013), based on recent receiver functions work the latter scenario is not plausible to explain the null pattern in central Norway since no deep thermal anomaly was found which may be a driver for upwelling beneath the Scandes (Makushkina et al., 2019). Furthermore, for deformation related to the Caledonian orogeny one would expect a fast axis orientation that is nearly parallel to the strike of the present Scandinavian mountain chain (e.g. Vauchez & Nicolas, 1991; Silver, 1996). Only a few stations located along the western coast of Norway show such a NE-SW orientation for ϕ. In contrast, for stations north of 65°N, ϕ is consistently aligned in NE-SW direction across different tectonic domains from the Lofoten Islands in the northwest to the Bothnian Sea in the southeast. However, if we assume that each of the measured nulls resulted from waves arriving from backazimuth directions parallel to the strike of the Scandes, the consistently observed null patterns at neighboring stations would indicate a ϕ orientation in NE-SW direction, parallel to the mountain chain (**Fig. S17**). Thus, although no clear orogen-parallel fast axis is measured for the southern region (except the nulls), an influence of the Caledonian collision (which represents the last major tectonic event) is most plausible to explain the splitting observations.

6.1.3 Northern Norway and Sweden (65°N - 71°N)

The most robust feature constrained by the modeling is a dipping symmetry axis geometry below stations mainly located on the Paleoproterozoic domain (purple area) with a dip towards NE by angles of 60° to 70° (Fig. 9). This result is generally consistent with the results of Eken et al. (2010) for the most northern stations of the SNSN. Furthermore, anisotropy beneath the Paleoproterozoic domain was analyzed previously in the framework of the LAPNET project: While Plomerová et al. (2011) indicated spatial variability of anisotropic fabrics related to different tectonic blocks, Vinnik et al. (2014) found evidence for multi-layered anisotropy in different depths ranges. Since the consistent dip pattern from our modeling is observed across a widespread area (Fig. 9), two scenarios are plausible to explain a dip of the fast axis. The first is based on the assumption that the measured anisotropic signature (with dipping symmetry axis) was already imprinted into the whole lithosphere long before the formation of the Baltic Shield during the phase of craton building (Fig.

11a). Alternatively, several episodes of collision and subduction "transformed" the previously horizontal fast axis to a dipping one by inclining its orientation as a result of multiple underthrusting events (Fig. 11b). Such a model was proposed by Babuška et al. (1993) to explain the growth of cratons and continents. A real-case scenario can be found in the Gulf of Bothnia at around 64°N, where a NE-dipping reflector was constrained from seismic reflection data in the framework of the BABEL project (BABEL Working Group, 1990; Balling, 2000; Korja & Heikkinen, 2005, see S1 in Fig. 1). This inclined reflector was interpreted as a remnant of a paleo-subduction system. The reflection profile only enables a 2D view on this area and the lateral extension of the reflector and the average dip-angle are not well-resolved (Balling, 2000). However, the inferred NE-ward dip coincides with our modeled fast-splitting direction.

Large-scale layering beneath Fennoscandia, indicative for several tectonic collision regimes, was inferred by receiver function analysis. Compared to other areas of (active) subduction processes like the Tibetan Plateau and the Himalayas, the likely signatures of ancient subduction zones beneath Fennoscandia cannot be clearly resolved so far (Kind et al., 2013). Nevertheless, recent work based on *S*-wave receiver functions from the Canadian Shield supports this hypothesis and presumes that dipping mid-lithospheric layers may be a general characteristic of old shield areas (Miller & Eaton, 2010). Therefore, the steeply dipping symmetry axes, observed consistently within a widespread area in northern Sweden, are a likely candidate to explain accretion due to several episodes of paleo-subduction.

In contrast to previous studies in Fennoscandia (Eken et al., 2010; Plomerová et al., 2011), the dipping symmetry axes, however, can be clearly constrained from shear-wave splitting measurements alone. Globally such observations are rare (e.g. Hartog & Schwartz, 2000; Liddell et al., 2017) since the characterization of the indicative splitting pattern depends on sufficient data coverage. Otherwise slight variations between only few observations can be misinterpreted as uncertainties in the splitting measurements.

6.1.4 Finland

The Paleoproterozoic domain is also traversed by the Baltic Bothnian megashear zone (BBZ, Fig. 1) which runs in N-S direction nearly parallel to the national border between Sweden and Finland (Berthelsen & Marker, 1986). Splitting signatures related to deformation from the active episodes of the BBZ could be either a ϕ orientation parallel to the strike of the shear zone (roughly N-S) or at least a contrast in splitting properties across the shear zone (e.g. Chevrot et al., 2004). Neither is observed directly at the BBZ (Fig. 1). A N-S oriented ϕ parallel to the BBZ is only found for stations located northeast and east of the BBZ, mainly on the Archean domain (red in Fig. 1). Similar orientations for ϕ as ours were also measured by Vinnik et al. (2014). The NNE-trending pattern observed for the region east of the BBZ is equivalent to the rest of the Paleoproterozoic domain and, therefore, the measured shear-wave splitting is likely not related to the BBZ. In contrast, the consistent NNE-SSW orientation of ϕ at the sparse number of stations on the Archean domain is well constrained based on mostly long recording periods at the corresponding permanent stations (see **Fig. S16** in the Supporting Information, e.g. the most eastern station JOF). Therefore, this sharp contrast for the orientation of ϕ relative to areas west of about 27°-28° again indicates that laterally different fabrics (related to the different tectonic units) are causing the change in the observed splitting pattern.

The most complex area to interpret is the Finnish part of the Svecofennian domain (Fig. 9). In the past shear-wave splitting was studied together with *P*-residuals in this area. The observations were mostly modeled with a dipping symmetry of anisotropy that varies between different tectonic blocks (Plomerová et al., 2006; Vecsey et al., 2007). Compared to our measurements at mostly long-running permanent stations, earlier studies were based on recordings of the dense temporary deployment SVEKALAPKO with only seven events of sufficient quality for a splitting analysis (Vecsey et al., 2007). Although the lateral resolution here is worse than for the dense SVEKALAPKO array, at several recording stations we were able to analyze data of partly more than ten years of observation compared to a maximum of five months of data recorded during the temporary SVEKALAPKO deployment. This allowed us to constrain the lateral anisotropic pattern with shear-wave splitting measurements alone. While for the northern area the *a*-axis dip towards NE is similar to Vecsey et al. (2007), for the central part of Finland we partly observe more complex splitting characteristics (Fig. 9, red circles and **Fig. S16** in the Supporting Information) which only in parts agree with the findings of Plomerová et al. (2006) and Vecsey et al. (2007).

In Fig. 12 we show exemplary modeling results for station KEF. While the ϕ values indicate a distinct jump at a backazimuth of 45°, the delay times δt are almost constant and do not have a clear periodicity over backazimuth which would be expected for a two-layer model with horizontal symmetry axes. The best model based on a combined ϕ-δt-fit (ϕ_{upp} = 30°, ϕ_{low} = 80°, δt_{upp} = 0.4 s, δt_{low} = 1.0 s) can explain the observed splitting pattern only in parts which is most clearly seen when comparing the stereoplots of observed and synthetic parameters computed from the best model (Fig. 12c-d). For a ϕ-only-fit (the RMSE calculated for the delay times is not taken into account to find the best-fit models) the splitting is best explained by a two-layer model with fast axis directions of 50° in the upper and $-80°$ in the lower layer (Fig. 12h). As expected the model fits the ϕ pattern quite well but the corresponding predicted delay times are much too high (δt_{upp} = 3 s and δt_{low} = 3.4 s) and do not fit the observations (with an average δt of $\sim$ 1.2 s) at all. A similar procedure was previously applied by Marson-Pidgeon & Savage (2004) for observations at station SNZO in New Zealand. Equally to our findings no significant variations of the delay times were measured while ϕ showed indications for a clear periodicity with respect to the incoming polarization directions. In order to explore if the complex splitting pattern at KEF can be explained by a dipping symmetry axis (at least in parts), additionally we performed a model search in this parameter space for the limited observed backazimuthal range assuming lateral variations in anisotropy. The results are summarized in Fig. 12i-l. The best model fits the observed δt values in principle quite well and also the locations of nulls show good agreement between synthetic and observed values. In contrast, ϕ can only be reconstructed in parts and the jump in the data between backazimuths of 45° and 65° is not explained by the model. However, the down-dip direction and the dip angle are well-constrained based on the 20 best-fit models. To summarize: although the data coverage in the northeastern quadrant is sufficient, it is neither possible to fully explain the observations (ϕ and δt) with a dipping layer nor a two-layer scenario. However, few surrounding stations are robustly modeled with a dip of the *a*-axis that is similar to the observations north of 65°N (Fig. 9). This suggests that also lateral variations of anisotropy around the individual stations may play a role. The previously documented lateral variations of the splitting parameters across the contact zone between the Paleoproterozoic Svecofennian domain and the Archean basement (Vecsey et al., 2007) cannot be resolved with the station distribution of ScanArray.

6.2 May (regional) lateral variations or deep anisotropy play a role?

In order to examine if lateral variations of anisotropy at regional scale could be responsible for the complex backazimuthal pattern observed at some recording stations in southern Finland, we compare the locations of raypath pierce points in different depth intervals down to 600 km depth (Fig. 13). This allows us to search for potential overlaps and areas in which all pierce points or raypaths sample the same volume.

The five station stereoplots shown in Fig. 13 (for their locations see red circles in Fig. 9) share the characteristic of a sharp rotation of ϕ from around $50°$-$60°$ (blue) to $0°$-$20°$ (greenish) within a narrow backazimuthal range of less than 5° in the NE quadrant. Measured delay times are almost constant except for station VAF and partly RAF at which significantly smaller values are observed. To explain such an abrupt change to be caused at shallow depths ($< 300\,\mathrm{km}$) it would require that around each single station the same lateral variation occurs for nearly the same azimuths. Stations KAF and KEF are located only $50\,\mathrm{km}$ apart from each other. Therefore, such small-scale variations (with almost identical splitting pattern) are quite unlikely (Fig. 13). For larger depths ($\geq 400\,\mathrm{km}$) the pierce point locations related to different stations partly overlap. In the presence of lateral variability in anisotropy one would therefore expect similar splitting characteristics for closely spaced pierce point locations, which is obviously not the case. Thus, the nearly identical ϕ-pattern at the five stations as well as the abrupt rotation of the fast axis are generally more indicative for a two- or multi-layer scenario than for laterally varying structure around each station (although the data coverage is mainly limited to the northeastern quadrant in a stereoplot view). At this point, in principal also the Fresnel zones of the different waves need to be considered to argue more about the finite-frequency sensitivity. However, the Fresnel zones of the individual waves (width $\sim$ 100-

200 km for dominant periods of $8\,\mathrm{s}$) at a single station largely overlap down to $500\,\mathrm{km}$ depth (e.g. Alsina & Snieder, 1995; Favier & Chevrot, 2003). Therefore, the significant change in ϕ cannot be explained with finite-frequency effects at all.

The main contributions to the anisotropy observations are most likely associated with fabrics in the lithosphere. However, the possibility that other sources of anisotropy, not related to the structure directly beneath Fennoscandia, can contribute to a complex splitting pattern has to be considered, too. Especially at the long-running permanent stations KAF, KEF and PVF clearly discrepant *SKS-SKKS* pairs were observed for the backazimuthal range in which the fast axes differ by around 80° (Grund & Ritter, 2019). Therefore, we cannot rule out that further contributions from the lowermost mantle are included in the splitting observations, although the discrepant pairs themselves were excluded before the modeling. In this case the poorly resolved orientation of ϕ from anisotropy in the lowermost mantle may contaminate the shallower signatures (e.g. Lynner & Long, 2012). This limitation is also interesting since some surrounding stations show slightly different splitting patterns which can be modeled by a dipping symmetry axis.

In order to check, if the observed delay times require an additional source beneath the lithosphere, following Helffrich (1995) a corresponding thickness L of an anisotropic layer can be estimated using

$$L \approx \frac{\delta t \cdot v_S}{\mathrm{d}v_S}, \tag{2}$$

where δt is the observed delay time, v_S is the isotropic shear-wave velocity and $\mathrm{d}v_S$ is the average percentage of anisotropy. The observed delay times at KEF, for instance, vary between 1 s and 1.5 s for the northeastern quadrant. In the mantle beneath stations in southern Finland, v_S is in the range of around 4.8 km/s (Pedersen et al., 2006; Vinnik et al., 2016). Taking these values and a $\mathrm{d}v_S$ of 4% as the upper limit for the strength of anisotropy prevalent in the upper 200 km of the Earth (Savage, 1999), the corresponding layer thickness varies between 120 km and 180 km. However, a lower percentage of anisotropy would result in an increased layer thickness. This trade-off cannot be modeled reliably and therefore a contribution from a deep source as inferred by discrepant *SKS* and *SKKS* phases may be most likely.

Moreover, the comparison of high-quality recordings of a single event from ENE backazimuth across stations in southern Finland shows a significant decrease of δt from east (δt =1.5 s at station JOF) to west (almost null at RAF) while ϕ is almost constant (Fig. 14). Thus, assuming a constant strength of anisotropy in the lithosphere beneath southern Finland, potentially an anisotropic layer of decreasing thickness from east to west should be located in this area.

6.3 Comparison with surface wave data and absolute plate motion

The observation of split core-refracted shear-waves indicates that anisotropy is located somewhere between the core-mantle boundary and the receiver at the surface. Thus, the depth estimation of the source of anisotropy cannot be determined from splitting measurements alone. In contrast to core-refracted shear-waves, surface waves have a much better depth resolution, however, their lateral resolution is usually limited due to the long wavelengths (partly $>$ 200 km). Therefore, estimates of azimuthal seismic anisotropy deduced by surface-wave analysis on a regional (e.g. Zhu & Tromp, 2013) or global scale (e.g. Becker et al., 2012; Schaeffer et al., 2016) mostly resolve smooth variations across different areas since the waves potentially sample portions of different anisotropic fabrics. Nevertheless, large-scale variations in anisotropy may also be resolved in shear-wave splitting measurements, provided that a dense, large-aperture station network is available. Despite partly strong variations of the splitting parameters with backazimuth and indications for a dipping symmetry axis, a comparison of the observations obtained from both approaches can be used to find similarities and/or discrepancies and may finally help to constrain an approximate depth range for the anisotropy beneath Fennoscandia.

A recent azimuthally anisotropic model based on adjoint tomography impressively reveals high correlations between the observed anisotropy and large-scale tectonic features in Europe and the North Atlantic (Zhu & Tromp, 2013; Zhu et al., 2015). Fig. 15 shows anisotropy fast axis orientations and strengths determined from surface wave data for Fennoscandia in four different depth ranges together with our best-fit models received from the splitting analysis. For depths of 100 km and beyond the fast axis directions (blue bars) are relatively constant for individual regions and provide only variations of the peak-to-peak amplitudes. The dominant trends from surface waves generally show high correlations with the splitting results, especially for the nearly NE-SW directions observed for parts of the Caledonides and the rotation of the fast axis towards a NW-SE direction parallel to the STZ in the most southern part of the study region. The upper layer fast axis orientation of the discussed two-layer model for station KONO (Fig. 10) also fits into this pattern while the possible ϕ orientation of the lower layer is not resolved by the surface wave data for the displayed depth ranges.

Weak anisotropy is consistently observed for all depth ranges in the area of the southern Caledonian nappes that is dominated by null splits (white circles with black edges) confirming the previously discussed possibility of partly isotropic fabrics in the crust and lithosphere. Thus, an alternative scenario of two layers with orthogonal symmetry axes and similar strengths resulting in apparent null splits can also be ruled out with high probability.

Due to the high correlation of the fast axis orientations in the western part of the study region (west of $\sim 21°$E), the peak in anisotropy strength allows to locate the main sources responsible for the shear-wave splitting in a depth interval of 70 km to 170 km (Fig. 15). Due to general agreement between splitting estimates from phases that were converted from *P*-to-*S* at the 410 km discontinuity (Olsson, 2007) and measurements from core-refracted phases, Eken et al. (2010) suggest that anisotropy beneath the SNSN stations is located shallower than 410 km. The lithosphere-asthenosphere boundary beneath Fennoscandia is located in depths of 200-250 km (e.g. Plomerová et al., 2002b; Artemieva, 2006). Therefore, most of the anisotropy is likely located in the lithospheric lower crust and uppermost mantle what supports the idea of fossil frozen-in anisotropy.

Another component which can cause anisotropy is the LPO of mantle minerals like olivine due to asthenospheric mantle flow (e.g. Zhang & Karato, 1995; Silver, 1996). As already shown in the histogram distributions in Fig. 5, the fast axis orientations observed across Fennoscandia align only in parts with the current absolute plate motion direction (APM) in a hotspot reference frame (HS3-NUVEL 1A, Gripp & Gordon, 2002). For a plate motion coupled to mantle flow one would expect a smoothly varying ϕ pattern across the network (e.g. Fouch et al., 2000) and no abrupt changes in ϕ within relatively small distances. The plate motion of the Baltic Shield is only around 1-1.5 cm per year and thus too slow to generate a dominant APM-parallel fabric caused by the motion of the plate across a sub-lithospheric shearing layer (Debayle & Ricard, 2013). Furthermore, especially for the Caledonian area, APM direction and orientations of expected anisotropy imprints caused by the continent-continent collision are almost identical. Compared to other continental areas like North America (e.g. Yang et al., 2014; Chen et al., 2018) or the easternmost regions of the East European Platform (Levin et al., 1999) we exclude asthenospheric flow as a primary cause for the observed anisotropy in the western part of Fennoscandia.

In contrast, based on a regional surface-wave study, asthenospheric flow not aligned with the APM direction was inferred for central and southern Finland below 200-250 km depth while no strong indicators for lithospheric contributions were found (Pedersen et al., 2006). The absence of a clear correlation with the APM was interpreted as complex flow pattern that cannot be explained by a scenario in which the Baltic Shield is coupled to the convecting mantle in a simple way. Our derived fast axes orientations are N-NE (0° - 40°) and generally agree with previous body wave observations which located the anisotropy mainly in the lithospheric mantle (Plomerová et al., 2006; Vecsey et al., 2007). Furthermore, the fast axis orientations of the surface wave model of Zhu & Tromp (2013) also show a similar pattern, although, only within the upper 70 km depth whereas below the fast axes rotate to the previously mentioned E-W direction that is consistent for deeper layers (Fig. 15). These models would be in clear contradiction with a nearly N-S aligned sub-lithospheric flow direction causing LPO. In the analyzed shear-wave splitting data of ScanArray such N-S orientation is only observed for the most eastern and northern parts of the study region (Archean domain). Although the proposed two-layer model for KEF, based on a combined ϕ-δt-fit (Fig. 12), cannot explain all the observations equally well, the orientation of ϕ_{upp} sufficiently fits the surface wave data in the upper 100 km. Moreover, the rotation of the fast axis into a nearly E-W direction for larger depths coincides with the orientation ϕ_{low} of the lower layer.

Due to the limited depth sensitivity of the surface waves, the strength of anisotropy decreases below 200 km (Zhu & Tromp, 2013). Thus, another N-S oriented component, related to flow in the asthenosphere, beneath 200 km depth cannot be ruled out (Pedersen et al., 2006). Nevertheless, although the lateral resolution of the surface-wave model of Zhu & Tromp (2013) is poor compared to the splitting measurements conducted at the individual stations, it supports the findings of complex anisotropic structure beneath that area. Dipping structures as found for several stations with *SKS* modeling, however, cannot be resolved by the used surface wave model parameterization (Zhu & Tromp, 2013).

Considering the observations and interpretations of the previous sections, in Fig. 16 we present our preferred anisotropy model for the area of southern Finland. While in the east, e.g. at station JOF, the simple splitting pattern can be explained by a single layer with horizontal fast axis direction (ϕ = 16°), the best two-layer model setting at station KEF (Fig. 12) indicates ϕ_{upp} = 30° for the upper layer and ϕ_{low} = 80° for the lower one. Including the observations of decreasing δt from east to west highlighted in Fig. 14 while ϕ is almost in the same direction at all stations, as well as the anisotropy model of Zhu & Tromp (2013) our preferred model consists of two layers in the west with an increase in thickness of the upper layer to the east.

7 CONCLUSIONS

Our shear-wave splitting measurements, analyzed at the dense and large-aperture ScanArray network across the Fennoscandian Peninsula, suggest a laterally complex anisotropic structure beneath Fennoscandia that partly correlates well with past tectonic activity. The observed splitting characteristics at several recording stations can be modeled reliably only with a dipping symmetry axis. Indicative one- and two-layer model characteristics mostly cannot fit the variations of the splitting parameters with backazimuth equally well or the models have a non-unique character. However, it has to be mentioned that the backazimuthal data coverage is partly limited due to the uneven distribution of global seismicity. In contrast to previous studies, where few splitting observations were jointly inverted with *P*-wave residuals, at several stations we can clearly resolve a dipping symmetry axis from shear-wave splitting measurements alone. Although the modeling constraints benefit from long recording periods at several stations, also data from temporary stations (mostly in neighboring areas around the permanent ones) with shorter recording times are robustly modeled by a dipping anisotropic fabric. However, short recording periods with only few measurements tempt analysts to perform simple averaging of individual ϕ and δt values. Thus, small variations due to dipping symmetry axes may be misinterpreted as measurement uncertainties. Therefore we suggest to run seismic stations (if possible) in the best case for more than 10 years, especially to perform meaningful modeling based on shear-wave splitting observations. The inferred dipping fabrics across Fennoscandia support assumptions that also old cratonic cores were formed by accretion as a consequence of repeated subduction events as indicated in Fig. 11.

ACKNOWLEDGMENTS

All individual single-event splitting measurements are available in electronic form via KITopen-data (Grund, 2019a, for further details see the Supporting Information). Multi-event results are listed in Table **S2** of the Supporting Information.

This work has received funding from the Deutsche Forschungsgemeinschaft (DFG) under the LITHOS-CAPP project (grants RI1133/11-1 and RI1133/11-1). Seismic instruments for the German contribution to ScanArray were kindly provided by the Geophysical Instrument Pool Potsdam (GIPP, Grund et al., 2017a). Logfiles of LITHOS-CAPP stations are available at the GFZ German Research Center for Geosciences online (Grund et al., 2017b). We thank Werner Scherer, Alexandra Mauerberger, Thomas Zieke, Lars Kilian, Benjamin Heit, Hanna Silvennoinen, Jouni Nevalainen, Henrik Jänkavarra, Andreas Björk, Joanna Holmgren and Sara Andersson for their support during the LITHOS-CAPP field work. The following institutions have contributed to the operation of the ScanArray network and made this study possible: University of Copenhagen, University of Oslo, University of Aarhus, GeoForschungsZentrum Potsdam (GFZ) and Karlsruhe Institute of Technology (KIT).

Data of stations from the following networks were used: 1) archived at GEOFON: 1G (ScanArray Core, Thybo et al., 2012; Grund et al., 2017a), 2D (Neonor2, Gradmann et al., 2014), DK (Danish National Seismic Network), EE (Estonian Seismological Network), FN (Northern Finland Seismological Network), HE (Finnish National Seismic Network), GE (GEOFON Program GFZ Potsdam, GEOFON Data Centre, 1993). 2) archived at ORFEUS (Dost, 1994): UP (Swedish National Seismic Network, SNSN, 1904), NS (Norwegian National Seismic Network, NNSN, 2017), NO (NORSAR). 3) archived at SEIS-UK (Brisbourne, 2012): ZR (SCANLIPS3D, England et al., 2015). 4) archived at KArlsruhe BroadBand Array (KABBA) Data Centre (`http:`

//gpikabba.gpi.kit.edu): Z6 (MAGNUS, Weidle et al., 2010). 5) archived at IRIS: II (IRIS/IDA Seismic Network, International Federation of Digital Seismograph Networks, 1986), IU (Global Seismograph Network, International Federation of Digital Seismograph Networks, 1993). Additional (partly restricted) data for the network codes HE, NS and UP were kindly provided by Universities of Helsinki (special thanks to Timo Tiira), Bergen and Uppsala.

Figures were prepared using Generic Mapping Tools (GMT and PyGMT, Wessel et al., 2013; Uieda et al., 2020), MATLAB® and Inkscape (v0.92). Digitized map contents included in Fig. 1 (tectonic units, deformation zones and inferred paleo-subduction zones) as well as Jupyter notebooks for reproduction of some of the figures generated with PyGMT are available from M. G.'s GitHub account (https://github.com/michaelgrund/GMT-plotting). MATLAB functions to reproduce modeling results can be downloaded from https://github.com/michaelgrund/sws_tools.

Abundant helpful comments and suggestions on the manuscript by Thomas Hertweck, Tuna Eken and an anonymous reviewer are acknowledged.

Supporting Information

Supplementary data are available at GJI online.

References

Alsina, D. & Snieder, R., 1995. Small-scale sublithospheric continental mantle deformation: Constraints from SKS splitting observations, *Geophys. J. Int.*, **123**, 431–448.

Aragon, J. C., Long, M. D., & Benoit, M. H., 2017. Lateral variations in SKS splitting across the MAGIC array, central Appalachians, *Geochem. Geophys. Geosyst.*, **18**, 4136–4155, doi:10.1002/2017GC007169.

Artemieva, I. M., 2006. Global 1×1 thermal model TC1 for the continental lithosphere: implications for lithosphere secular evolution, *Tectonophysics*, **416**, 245–277.

BABEL Working Group, 1990. Evidence for early Proterozoic plate tectonics from seismic reflection profiles in the Baltic shield, *Nature*, **348**, 34.

Babuška, V., Plomerova, J., & Šílenỳ, J., 1993. Models of seismic anisotropy in the deep continental lithosphere, *Phys. Earth Planet. In.*, **78**, 167–191.

Babuška, V. & Cara, M., 1991. *Seismic anisotropy in the Earth*, vol. 10, Kluwer Academic Publishers, Dordrecht, The Netherlands.

Balling, N., 2000. Deep seismic reflection evidence for ancient subduction and collision zones within the continental lithosphere of northwestern Europe, *Tectonophysics*, **329**, 269–300.

Barruol, G. & Hoffmann, R., 1999. Upper mantle anisotropy beneath the Geoscope stations, *J. Geophys. Res.*, **104**, 10757–10773.

Barruol, G. & Mainprice, D., 1993. A quantitative evaluation of the contribution of crustal rocks to the shear-wave splitting of teleseismic SKS waves, *Phys. Earth Planet. In.*, **78**, 281–300.

Becker, T. W., Lebedev, S., & Long, M. D., 2012. On the relationship between azimuthal anisotropy from shear wave splitting and surface wave tomography, *J. Geophys. Res.*, **117**, B01306.

Berthelsen, A., 1992. Mobile Europe, in *A Continent Revealed, The European Geotraverse*, pp. 11–32, Cambridge University Press.

Berthelsen, A. & Marker, M., 1986. 1.9-1.8 Ga old strike-slip megashears in the Baltic Shield, and their plate tectonic implications, *Tectonophysics*, **128**, 163–181.

Bird, P., 2003. An updated digital model of plate boundaries, *Geochem. Geophys. Geosyst.*, **4**, 1027.

Bowman, J. & Ando, M., 1987. Shear-wave splitting in the upper-mantle wedge above the Tonga subduction zone, *Geophys. J. Roy. Astron. Soc.*, **88**, 25–41.

Brisbourne, A., 2012. How to store and share geophysical data, *Astron. Geophys.*, **53**, 19–20.

Chen, X., Li, Y., & Levin, V., 2018. Shear wave splitting beneath eastern North American continent: evidence for a multi-layered and laterally variable anisotropic structure, *Geochem. Geophys. Geosyst.*, **19**, 2857–2871.

Chevrot, S., 2000. Multichannel analysis of shear wave splitting, *J. Geophys. Res.*, **105**, 21579–21590.

Chevrot, S., Favier, N., & Komatitsch, D., 2004. Shear wave splitting in three-dimensional anisotropic media, *Geophys. J. Int.*, **159**, 711–720.

Chew, D. M. & Strachan, R. A., 2014. The Laurentian Caledonides of Scotland and Ireland, *Geological Society, London, Special Publications*, **390**(1), 45–91.

Crampin, S. & Booth, D. C., 1985. Shear-wave polarizations near the North Anatolian Fault-II. Interpretation in terms of crack-induced anisotropy, *Geophys. J. Roy. Astron. Soc.*, **83**, 75–92.

Currie, C. A., Cassidy, J. F., Hyndman, R. D., & Bostock, M. G., 2004. Shear wave anisotropy beneath the Cascadia subduction zone and western North American craton, *Geophys. J. Int.*, **157**, 341–353.

Debayle, E. & Ricard, Y., 2013. Seismic observations of large-scale deformation at the bottom of fast-moving plates, *Earth Planet. Sci. Lett.*, **376**, 165–177.

Deng, J., Long, M. D., Creasy, N., Wagner, L., Beck, S., Zandt, G., Tavera, H., & Minaya, E., 2017. Lowermost mantle anisotropy near the eastern edge of the Pacific LLSVP: constraints from SKS-SKKS splitting intensity measurements, *Geophys. J. Int.*, **210**, 774–786.

Domeier, M., 2016. A plate tectonic scenario for the Iapetus and Rheic oceans, *Gondwana Research*, **36**, 275–295.

Dost, B., 1994. The ORFEUS Data Center, *Annals of Geophysics*, **37**.

Dziewoński, A. M., Chou, T.-A., & Woodhouse, J. H., 1981. Determination of earthquake source parameters from waveform data for studies of global and regional seismicity, *J. Geophys. Res.*, **86(B4)**, 2825–2852, doi:10.1029/JB086iB04p02825.

Eakin, C. M., Long, M. D., Scire, A., Beck, S. L., Wagner, L. S., Zandt, G., & Tavera, H., 2016. Internal deformation of the subducted Nazca slab inferred from seismic anisotropy, *Nature Geosci.*, **9**, 56–59.

Eken, T., Plomerová, J., Roberts, R., Vecsey, L., Babuška, V., Shomali, H., & Bodvarsson, R., 2010. Seismic anisotropy of the mantle lithosphere beneath the Swedish National Seismological Network (SNSN), *Tectonophysics*, **480**, 241–258.

Ekström, G., Nettles, M., & Dziewoński, A. M., 2012. The global CMT project 2004-2010: Centroid-moment tensors for 13,017 earthquakes, *Phys. Earth Planet. In.*, **200**, 1–9, doi:10.1016/j.pepi.2012.04.002.

England, R. W., Ebbing, J., & Ben Mansour, W., 2015. SCANLIPS3D - SCANdinavian LIthosphere P and S wave experiment 3 D, Scientific report 959, NERC Geophysical Equipment Facility.

Eugeno-S Working Group, 1988. Crustal structure and tectonic evolution european of the transition between the Baltic Shield and the North German Caledonides (the EUGENO-S Project), *Tectonophysics*, **150**, 253–348.

Favier, N. & Chevrot, S., 2003. Sensitivity kernels for shear wave splitting in transverse isotropic media, *Geophys. J. Int.*, **153**, 213–228.

Fouch, M. J. & Rondenay, S., 2006. Seismic anisotropy beneath stable continental interiors, *Phys. Earth Planet. In.*, **158**, 292–320.

Fouch, M. J., Fischer, K. M., Parmentier, E. M., Wysession, M. E., & Clarke, T. J., 2000. Shear wave splitting, continental keels, and patterns of mantle flow, *J. Geophys. Res.*, **105**, 6255–6275.

Fukao, Y., 1984. Evidence from core-reflected shear waves for anisotropy in the Earth's mantle, *Nature*, **309**, 695.

Gaál, G., 1986. 2200 million years of crustal evolution: the Baltic Shield, *Bull. Geol. Soc. Finland*, **58**, 149–168.

Gaál, G. & Gorbatschev, R., 1987. An outline of the Precambrian evolution of the Baltic Shield, *Precambrian Res.*, **35**, 15–52.

Gee, D. G., Fossen, H., Henriksen, N., & Higgins, A. K., 2008. From the early Paleozoic platforms of Baltica and Laurentia to the Caledonide Orogen of Scandinavia and Greenland, *Episodes*, **31**, 44–51.

GEOFON Data Centre, 1993. GEOFON (GeoForschungsNetz), Seismic Network, Deutsches GeoForschungsZentrum GFZ.

Gorbatchev, R., 2004. The Transscandinavian Igneous Belt – introduction and background, in *The Transscandinavian Igneous Belt (TIB) in Sweden: a Review of Its Character and Evolution. Geological Survey of Finland, Special Paper*, vol. 37, pp. 9–15, eds Högdahl, K., Andersson, U., & Eklund, O., Geological Survey of Finland.

Gradmann, S., Keiding, M., Olesen, O., & Maystrenko, Y., 2014. NEONOR2-Neotectonics in

Nordland, NW Norway, in *Eighth Symposium on Structure, Composition and Evolution of the Lithosphere in Fennoscandia*, p. 17.

Gregersen, S., Voss, P., & TOR Working Group, 2002. Summary of project TOR: delineation of a stepwise, sharp, deep lithosphere transition across Germany–Denmark–Sweden, *Tectonophysics*, **360**, 61–73.

Gripp, A. E. & Gordon, R. G., 2002. Young tracks of hotspots and current plate velocities, *Geophys. J. Int.*, **150**, 321–361.

Grund, M., 2017. StackSplit - a plugin for multi-event shear wave splitting analyses in SplitLab, *Comput. Geosci.*, **105**, 43–50, doi:10.1016/j.cageo.2017.04.015.

Grund, M., 2019a. Dissertation electronic appendix, KITopenData, doi:10.5445/IR/1000091427.

Grund, M., 2019b. *Exploring geodynamics at different depths with shear wave splitting*, Ph.D. thesis, Karlsruhe Institute of Technology (KIT), doi:10.5445/IR/1000091425.

Grund, M. & Ritter, J. R. R., 2019. Widespread seismic anisotropy in Earth's lowermost mantle beneath the Atlantic and Siberia, *Geology*, **47(2)**, 123–126, doi:10.1130/G45514.1.

Grund, M., Mauerberger, A., Ritter, J. R. R., & Tilmann, F., 2017a. Broadband Recordings for LITHOS-CAPP: LITHOspheric Structure of Caledonian, Archaean and Proterozoic Provinces Sep. 2014 - Oct. 2016, Sweden and Finland, Scientific Technical Report STR-Data 17/02, GIPP Experiment and Data Archive, Potsdam: GFZ German Research Centre for Geosciences, doi:10.2312/GFZ.b103-17029.

Grund, M., Mauerberger, A., Ritter, J. R. R., & Tilmann, F., 2017b. Broadband Recordings for LITHOS-CAPP: LITHOspheric Structure of Caledonian, Archaean and Proterozoic Provinces Sep. 2014 - Oct. 2016, Sweden and Finland, Recorder log-file - Datasets, GFZ Data Services, doi:10.5880/GIPP.201417.1.

Hall, S. A., Kendall, J.-M., & van der Baan, M., 2004. Some comments on the effects of lower-mantle anisotropy on SKS and SKKS phases, *Phys. Earth Planet. In.*, **146**, 469–481.

Hartog, R. & Schwartz, S. Y., 2000. Subduction-induced strain in the upper mantle east of the Mendocino triple junction, California, *J. Geophys. Res.*, **105**, 7909–7930.

Heeremans, M., Larsen, B. T., & Stel, H., 1996. Paleostress reconstruction from kinematic indicators in the Oslo Graben, southern Norway: new constraints on the mode of rifting, *Tectonophysics*, **266**, 55–79.

Helffrich, G., 1995. Lithospheric deformation inferred from teleseismic shear wave splitting observations in the United Kingdom, *J. Geophys. Res.*, **100**, 18195–18204.

Hicks, S. P., Nippress, S. E. J., & Rietbrock, A., 2012. Sub-slab mantle anisotropy beneath south-central Chile, *Earth Planet. Sci. Lett.*, **357**, 203–213.

International Federation of Digital Seismograph Networks, 1986. IRIS/IDA Seismic Network, Seismic Network, Scripps Institution of Oceanography.

International Federation of Digital Seismograph Networks, 1993. Global Seismograph Network (GSN – IRIS/USGS), Seismic Network, Albuquerque Seismological Laboratory (ASL)/USGS.

Kennett, B. L. N., 1991. IASPEI 1991 seismological tables, *Terra Nova*, **3(2)**, 122.

Kind, R., Gregersen, S., Hanka, W., & Bock, G., 1997. Seismological evidence for a very sharp Sorgenfrei-Tornquist zone (STZ) in southern Sweden, *Geological Magazine*, **134**, 591–595.

Kind, R., Sodoudi, F., Yuan, X., Shomali, H., Roberts, R., Gee, D., Eken, T., Bianchi, M., Tilmann, F., & Balling, N., 2013. Scandinavia: a former Tibet?, *Geochem. Geophys. Geosyst.*, **14**, 4479–4487.

Kong, F., Gao, S. S., & Liu, K. H., 2015. Applicability of the multiple-event stacking technique for shear-wave splitting analysis, *Bull. Seismol. Soc. Am.*, **105**, 3156–3166.

Korja, A. & Heikkinen, P., 2005. The accretionary Svecofennian orogen-insight from the BABEL profiles, *Precambrian Res.*, **136**, 241–268.

Korja, A., Lahtinen, R., & Nironen, M., 2006. The Svecofennian orogen: a collage of microcontinents and island arcs, *Geological Society, London, Memoirs*, **32**, 561–578, doi:10.1144/GSL.MEM.2006.032.01.34.

Krogh, E. J., 1977. Evidence of Precambrian continent-continent collision in Western Norway, *Nature*, **267**, 17.

Lahtinen, R., Korja, A., & Nironen, M., 2005. Paleoproterozoic tectonic evolution, in *Developments in Precambrian Geology*, vol. 14, pp. 481–531.

Larsen, B. T., Olaussen, S., Sundvoll, B., & Heeremans, M., 2008. The Permo-Carboniferous

Oslo Rift through six stages and 65 million years, *Episodes*, **31**(1), 52–58.

Lawver, L. A., Gahagan, L. M., & Norton, I., 2011. Palaeogeographic and tectonic evolution of the Arctic region during the Palaeozoic, in *Arctic Petroleum Geology*, Geological Society of London.

Levin, V., Menke, W., & Park, J., 1999. Shear wave splitting in the Appalachians and the Urals: a case for multilayered anisotropy, *J. Geophys. Res.*, **104**, 17975–17993.

Liddell, M. V., Bastow, I., Darbyshire, F., Gilligan, A., & Pugh, S., 2017. The formation of Laurentia: Evidence from shear wave splitting, *Earth Planet. Sci. Lett.*, **479**, 170–178.

Long, M. D. & Silver, P. G., 2009. Shear wave splitting and mantle anisotropy: Measurements, interpretations, and new directions, *Surv. Geophys.*, **30**, 407–461.

Lynner, C. & Bodmer, M., 2017. Mantle flow along the eastern North American margin inferred from shear wave splitting, *Geology*, **45**, 867–870, doi:10.1130/G38980.1.

Lynner, C. & Long, M. D., 2012. Evaluating contributions to SK(K)S splitting from lower mantle anisotropy: A case study from station DBIC, Côte D'Ivoire, *Bull. Seismol. Soc. Am.*, **102(3)**, 1030–1040.

Makushkina, A., Tauzin, B., Tkalčić, H., & Thybo, H., 2019. The Mantle Transition Zone in Fennoscandia: Enigmatic high topography without deep mantle thermal anomaly, *Geophys. Res. Lett.*.

Marson-Pidgeon, K. & Savage, M. K., 2004. Modelling shear wave splitting observations from Wellington, New Zealand, *Geophys. J. Int.*, **157**, 853–864.

Maupin, V., Agostini, A., Artemieva, I., Balling, N., Beekman, F., Ebbing, J., England, R. W., Frassetto, A., Gradman, S., Jacobsen, B. H., Köhler, A., Kvarnen, T., Medhus, A. B., Mjelde, R., Ritter, J., Sokoutis, D., Stratford, W., Thybo, H., Wawerzinek, B., & Weidle, C., 2013. The deep structure of the Scandes and its relation to tectonic history and present-day topography, *Tectonophysics*, **602**, 15–37.

McKerrow, W. S., Mac Niocaill, C., & Dewey, J. F., 2000. The Caledonian orogeny redefined, *Geological Society of London*, **157**, 1149–1154.

Medhus, A. B., Balling, N., Jacobsen, B. H., Kind, R., & England, R. W., 2009. Deep-structural differences in southwestern Scandinavia revealed by P-wave travel time residuals, *Norw. J. Geol.*, **89**.

Medhus, A. B., Balling, N., Jacobsen, B. H., Weidle, C., England, R. W., Kind, R., Thybo, H., & Voss, P., 2012. Upper-mantle structure beneath the Southern Scandes Mountains and the Northern Tornquist Zone revealed by P-wave traveltime tomography, *Geophys. J. Int.*, **189**, 1315–1334.

Miller, M. S. & Eaton, D. W., 2010. Formation of cratonic mantle keels by arc accretion: Evidence from S receiver functions, *Geophys. Res. Lett.*, **37**, 1–5, doi:10.1029/2010GL044366.

Mitchell, W. I., 2004. *The Geology of Northern Ireland: Our Natural Foundation*, Geological Survey of Northern Ireland, Belfast, Northern Ireland.

Mondal, P. & Long, M. D., 2019. A model space search approach to finite-frequency SKS splitting intensity tomography in a reduced parameter space, *Geophys. J. Int.*, **217**, 238–256.

Mondal, P. & Long, M. D., 2020. Strong seismic anisotropy in the deep upper mantle beneath the Cascadia backarc: Constraints from probabilistic finite-frequency SKS splitting intensity tomography, *Earth Planet. Sci. Lett.*, **539**, 116172.

Munzarová, H., Plomerová, J., Kissling, E., Vecsey, L., & Babuška, V., 2018. Novel anisotropic teleseismic body-wave tomography code AniTomo to illuminate heterogeneous anisotropic upper mantle: Part II - Application to data of passive seismic experiment LAPNET in northern Fennoscandia, *Geophys. J. Int.*, **215**, 1388–1409.

Murphy, J. B., Waldron, J. W. F., Schofield, D. I., Barry, T. L., & Band, A. R., 2014. Highly depleted isotopic compositions evident in Iapetus and Rheic Ocean basalts: implications for crustal generation and preservation, *Intern. Journ. Earth Sci.*, **103**(5), 1219–1232.

Nielsen, S. B., Gallagher, K., Leighton, C., Balling, N., Svenningsen, L., Jacobsen, B. H., Thomsen, E., Nielsen, O. B., Heilmann-Clausen, C., Egholm, D. L., Sunmmerfield, M. A., Clausen, O. R., Piotrowski, J. A., Thorsen, M. R., Huuse, M., Abrahamsen, N., King, C., & Lykke-Andersen, H., 2009. The evolution of western Scandinavian topography: a review of Neogene uplift versus the ICE (isostasy-climate-erosion) hypothesis, *J. Geodynamics*, **47**, 72–95.

NNSN, 2017. Annual report for the Norwegian National Seismic Network 2016, University of

Bergen, Bergen, Norway.

Olsson, S., 2007. *Analyses of seismic wave conversion in the crust and upper mantle beneath the Baltic Shield*, Ph.D. thesis, Acta Universitatis Upsaliensis.

Pedersen, H. A., Bruneton, M., & Maupin, V., 2006. Lithospheric and sublithospheric anisotropy beneath the Baltic shield from surface-wave array analysis, *Earth Planet. Sci. Lett.*, **244**, 590–605.

Pedersen, T., Gregersen, S., & TOR Working Group, 1999. Project Tor: deep lithospheric variation across the Sorgenfrei-Tornquist Zone, southern Scandinavia, *Bull. Geol. Soc. Denmark*, **46**, 13–24.

Pharaoh, T. C., 1999. Palaeozoic terranes and their lithospheric boundaries within the Trans-European Suture Zone (TESZ): a review, *Tectonophysics*, **314**, 17–41.

Plomerová, J., Arvidsson, R., Babuška, V., Granet, M., Kulhánek, O., Poupinet, G., & Šılenỳ, J., 2001. An array study of lithospheric structure across the Protogine zone, Värmland, south-central Sweden - signs of a paleocontinental collision, *Tectonophysics*, **332**, 1–21.

Plomerová, J., Babuška, V., Vecsey, L., & Kouba, D., 2002a. Seismic anisotropy of the lithosphere around the Trans-European Suture Zone (TESZ) based on teleseismic body-wave data of the TOR experiment, *Tectonophysics*, **360**, 89–114.

Plomerová, J., Kouba, D., & Babuška, V., 2002b. Mapping the lithosphere-asthenosphere boundary through changes in surface-wave anisotropy, *Tectonophysics*, **358**, 175–185.

Plomerová, J., Babuška, V., Vecsey, L., Kozlovskaya, E., & Raita, T., 2006. Proterozoic-Archean boundary in the mantle lithosphere of eastern Fennoscandia as seen by seismic anisotropy, *J. Geodynamics*, **41**, 400–410.

Plomerová, J., Vecsey, L., Babuška, V., Heikkinen, P., & Komminaho, K., 2011. Domains of Archean mantle lithosphere deciphered by seismic anisotropy-initial results from the LAPNET array in northern Fennoscandia, *Solid Earth*, **2**, 303–313, doi:10.5194/se–2–303–2011.

Rickers, F., Fichtner, A., & Trampert, J., 2013. The Iceland–Jan Mayen plume system and its impact on mantle dynamics in the North Atlantic region: evidence from full-waveform inversion, *Earth Planet. Sci. Lett.*, **367**, 39–51.

Roberts, D., 2003. The Scandinavian Caledonides: event chronology, palaeogeographic settings and likely modern analogues, *Tectonophysics*, **365**, 283–299.

Roy, C. & Ritter, J. R. R., 2013. Complex deep seismic anisotropy below the Scandinavian Mountains, *J. Seism.*, **17**, 361–384.

Savage, M. K., 1999. Seismic anisotropy and mantle deformation: what have we learned from shear wave splitting, *Rev. Geophys.*, **37**, 69–106.

Schaeffer, A. J., Lebedev, S., & Becker, T. W., 2016. Azimuthal seismic anisotropy in the Earth's upper mantle and the thickness of tectonic plates, *Geophys. J. Int.*, **207**, 901–933.

Silver, P. G., 1996. Seismic anisotropy beneath the continents: Probing the depths of geology, *Annu. Rev. Earth Planet. Sci.*, **24**, 385–432.

Silver, P. G. & Chan, W. W., 1991. Shear wave splitting and subcontinental mantle deformation, *J. Geophys. Res.*, **96**, 16429–16454.

Silver, P. G. & Savage, M. K., 1994. The interpretation of shear-wave splitting parameters in the presence of two anisotropic layers, *Geophys. J. Int.*, **119**, 949–963.

SNSN, 1904. SNSN (Swedish National Seismic Network), Seismic Network, Uppsala University, Uppsala, Sweden, doi:10.18159/SNSN.

Thybo, H., Balling, N., Maupin, V., Ritter, J., & Tilmann, F., 2012. ScanArray Core (1G 2012-2017), Seismic Network, The ScanArray consortium, doi:10.14470/6T569239.

Tian, X., Zhang, J., Si, S., Wang, J., Chen, Y., & Zhang, Z., 2011. SKS splitting measurements with horizontal component misalignment, *Geophys. J. Int.*, **185**, 329–340.

Torsvik, T. H. & Cocks, L. R. M., 2005. Norway in space and time: A Centennial cavalcade, *Norw. J. Geol.*, **85**.

Torsvik, T. H. & Rehnström, E. F., 2003. The Tornquist Sea and Baltica-Avalonia docking, *Tectonophysics*, **362**, 67–82.

Uieda, L., Tian, D., Leong, W. J., Toney, L., & Wessel, P., 2020. PyGMT: A Python interface for the Generic Mapping Tools, v0.1.0, Zenodo, doi:10.5281/zenodo.3782862.

Vauchez, A. & Nicolas, A., 1991. Mountain building: strike-parallel motion and mantle anisotropy, *Tectonophysics*, **185**, 183–201.

Vecsey, L., Plomerová, J., Kozlovskaya, E., & Babuška, V., 2007. Shear wave splitting as a diagnostic of variable anisotropic structure of the upper mantle beneath central Fennoscandia, *Tectonophysics*, **438**, 57–77.

Vinnik, L., Makeyeva, L. I., Milev, A., , & Usenko, A. Y., 1992. Global patterns of azimuthal anisotropy and deformations in the continental mantle, *Geophys. J. Int.*, **111**, 433–447.

Vinnik, L., Oreshin, S., Makeyeva, L., Peregoudov, D., & Kozlovskaya, E., 2014. Anisotropic lithosphere under the Fennoscandian shield from P receiver functions and SKS waveforms of the POLENET/LAPNET array, *Tectonophysics*, **628**, 45–54.

Vinnik, L., Kozlovskaya, E., Oreshin, S., Kosarev, G., Piiponen, K., & Silvennoinen, H., 2016. The lithosphere, LAB, LVZ and Lehmann discontinuity under central Fennoscandia from receiver functions, *Tectonophysics*, **667**, 189–198.

Walker, A. M. & Wookey, J., 2012. MSAT - a new toolkit for the analysis of elastic and seismic anisotropy, *Comput. Geosci.*, **49**, 81–90.

Walsh, E., Arnold, R., & Savage, M. K., 2013. Silver and Chan revisited, *J. Geophys. Res.*, **118**, 5500–5515.

Wawerzinek, B., 2012. *Untersuchung der elastischen Scherwellenstruktur unter dem Südskandinavischen Gebirge*, Ph.D. thesis, Karlsruhe Institute of Technology (KIT).

Wawerzinek, B., Ritter, J. R. R., & Roy, C., 2013. New constraints on the 3D shear wave velocity structure of the upper mantle underneath Southern Scandinavia revealed from non-linear tomography, *Tectonophysics*, **602**, 38–54.

Weidle, C., Maupin, V., Ritter, J., Kværna, T., Schweitzer, J., Balling, N., Thybo, H., Faleide, J. I., & Wenzel, F., 2010. MAGNUS-A Seismological Broadband Experiment to Resolve Crustal and Upper Mantle Structure beneath the Southern Scandes Mountains in Norway, *Seism. Res. Lett.*, **81(1)**, 76–84, doi:10.1785/gssrl.81.1.76.

Wessel, P., Smith, W. H. F., Scharroo, R., Luis, J., & Wobbe, F., 2013. Generic Mapping Tools: Improved version released, *Eos Trans. AGU*, **94(45)**, 409–420.

Wolfe, C. J. & Silver, P. G., 1998. Seismic anisotropy of oceanic upper mantle: Shear wave splitting methodologies and observations, *J. Geophys. Res.*, **103**, 749–771.

Wüstefeld, A. & Bokelmann, G., 2007. Null detection in shear-wave splitting measurements, *Bull. Seismol. Soc. Am.*, **97(4)**, 1204–1211.

Wüstefeld, A., Bokelmann, G., Zaroli, C., & Barruol, G., 2008. SplitLab: A shear-wave splitting environment in Matlab, *Comput. Geosci.*, **34**, 515–528.

Wüstefeld, A., Bokelmann, G., & Barruol, G., 2010. Evidence for ancient lithospheric deformation in the East European Craton based on mantle seismic anisotropy and crustal magnetics, *Tectonophysics*, **481**, 16–28.

Wylegalla, K., Bock, G., Gossler, J., & Hanka, W., 1999. Anisotropy across the Sorgenfrei-Tornquist Zone from shear wave splitting, *Tectonophysics*, **314**, 335–350.

Yang, B. B., Gao, S. S., Liu, K. H., Elsheikh, A. A., Lemnifi, A. A., Refayee, H. A., & Yu, Y., 2014. Seismic anisotropy and mantle flow beneath the northern Great Plains of North America, *J. Geophys. Res.*, **119**, 1971–1985.

Yuan, K. & Beghein, C., 2014. Three-dimensional variations in Love and Rayleigh wave azimuthal anisotropy for the upper 800 km of the mantle, *J. Geophys. Res.*, **119**, 3232–3255.

Zhang, S. & Karato, S.-I., 1995. Lattice preferred orientation of olivine aggregates deformed in simple shear, *Nature*, **375**, 774.

Zhu, H. & Tromp, J., 2013. Mapping tectonic deformation in the crust and upper mantle beneath Europe and the North Atlantic Ocean, *Science*, **341**, 871–875.

Zhu, H., Bozdağ, E., & Tromp, J., 2015. Seismic structure of the European upper mantle based on adjoint tomography, *Geophys. J. Int.*, **201**, 18–52.

Zielhuis, A. & Nolet, G., 1994. Deep seismic expression of an ancient plate boundary in Europe, *Science*, **265**, 79–81.

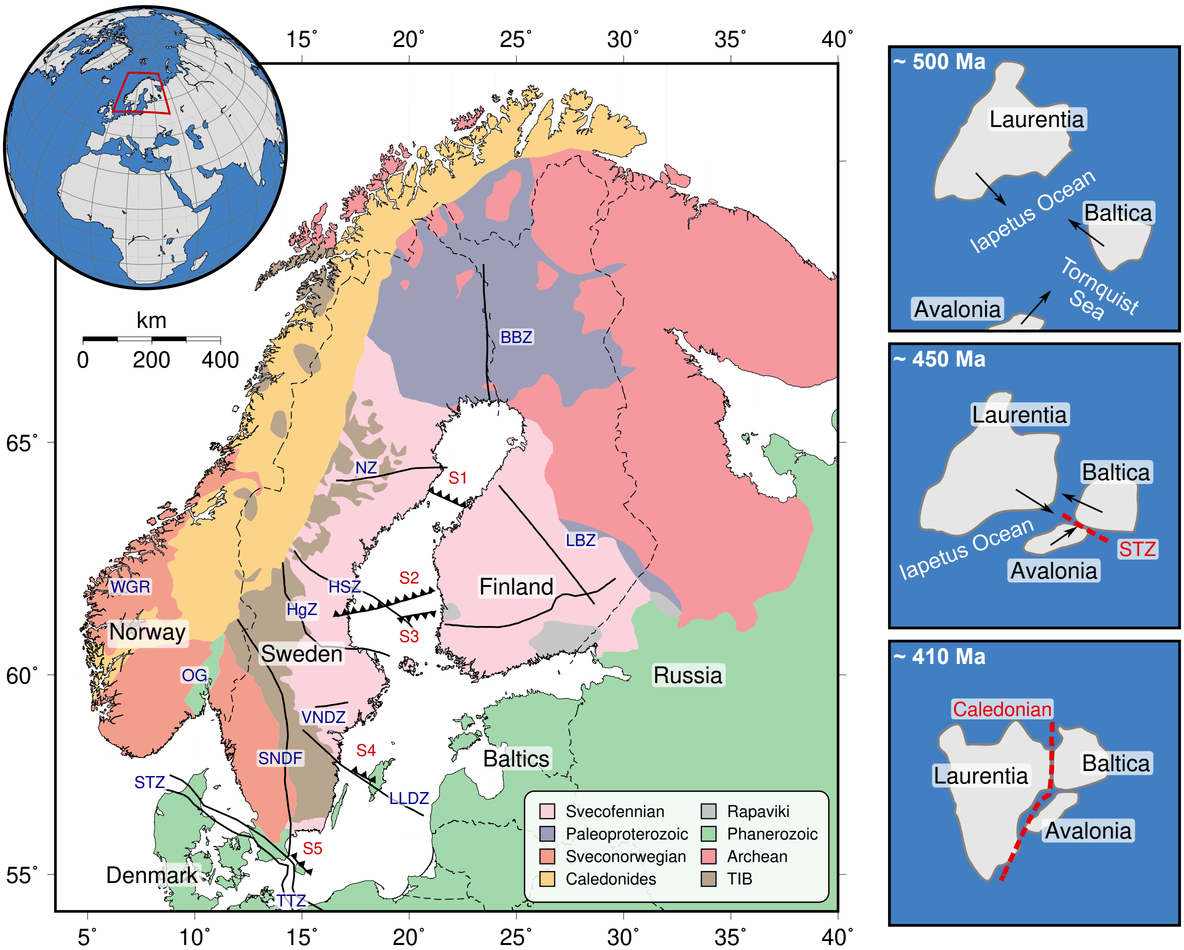

Figure 1. Left: Simplified geological/tectonic map of Fennoscandia and surrounding areas after Gorbatchev (2004) and Korja & Heikkinen (2005). Locations of deformation zones (sutures, shear zones) are shown as black lines, inferred subduction zones based on reflection seismic data are indicated by black "sawtooth" lines with the pike pointing into the assumed subduction direction. Abbreviations (blue and red labels): *BBZ*, Baltic Bothnian megashear zone; *HgZ*, Hagsta deformation zone; *HSZ*, Hassela shear zone; *LBZ*, Ladoga-Bothnian Bay zone; *LLDZ*, Loftahammar, Linköping deformation zone; *NZ*, Nickel zone; *OG*, Oslo Graben; *S1-S5*, inferred subduction zones; *STZ*, Sorgenfrei-Tornquist Zone; *SNDF*, Sveconorwegian deformation zone; *TTZ*, Teisseyre-Tornquist Zone; *VNDZ*, Vingåker-Nyköping deformation zone; *WGR*, Western Gneiss Region. *TIB* stands for Transscandinavian Igneous Belt. Dashed black lines indicate national borders. Right: Simplified schematic after Mitchell (2004), Lawver et al. (2011), Chew & Strachan (2014), Murphy et al. (2014) and Domeier (2016) showing the evolution of Fennoscandia (and surrounding areas) in the context of plate tectonics (for details, see text).

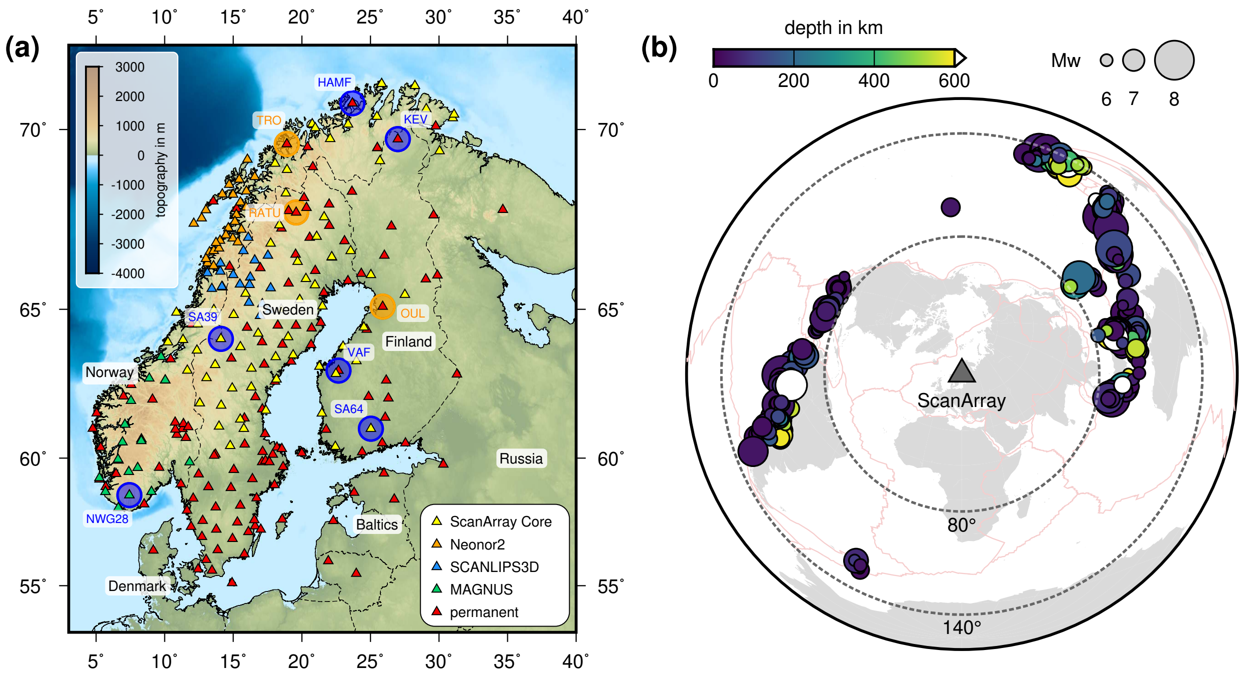

Figure 2. (**a**) Distribution of seismic recording stations used in the shear-wave splitting analysis. Color fill of the triangles indicates the different temporary (Weidle et al., 2010; Thybo et al., 2012; Gradmann et al., 2014; England et al., 2015; Grund et al., 2017a) and permanent seismic station deployments that form the extended ScanArray network. Dashed lines indicate national borders. The nine recording stations marked with blue (HAMF, KEV, NWG28, SA39, SA64 and VAF) and orange (OUL, TRO and RATU) circles are shown in detail in Fig. 6 and Fig. 8, respectively. (**b**) Distribution of 541 teleseismic earthquakes based on the Global CMT catalog (Dziewoński et al., 1981; Ekström et al., 2012) that yielded at least one *good*/*fair* split or null measurement. Color fill of the individual circles indicates the event depth and the size of the circles scales with the moment magnitude M_W. The epicentral distance window between 80° and 140° is displayed by the two dashed circles centered at the location of the ScanArray network (dark gray triangle). Landmasses are shown in gray and light red lines indicate plate boundaries after Bird (2003).

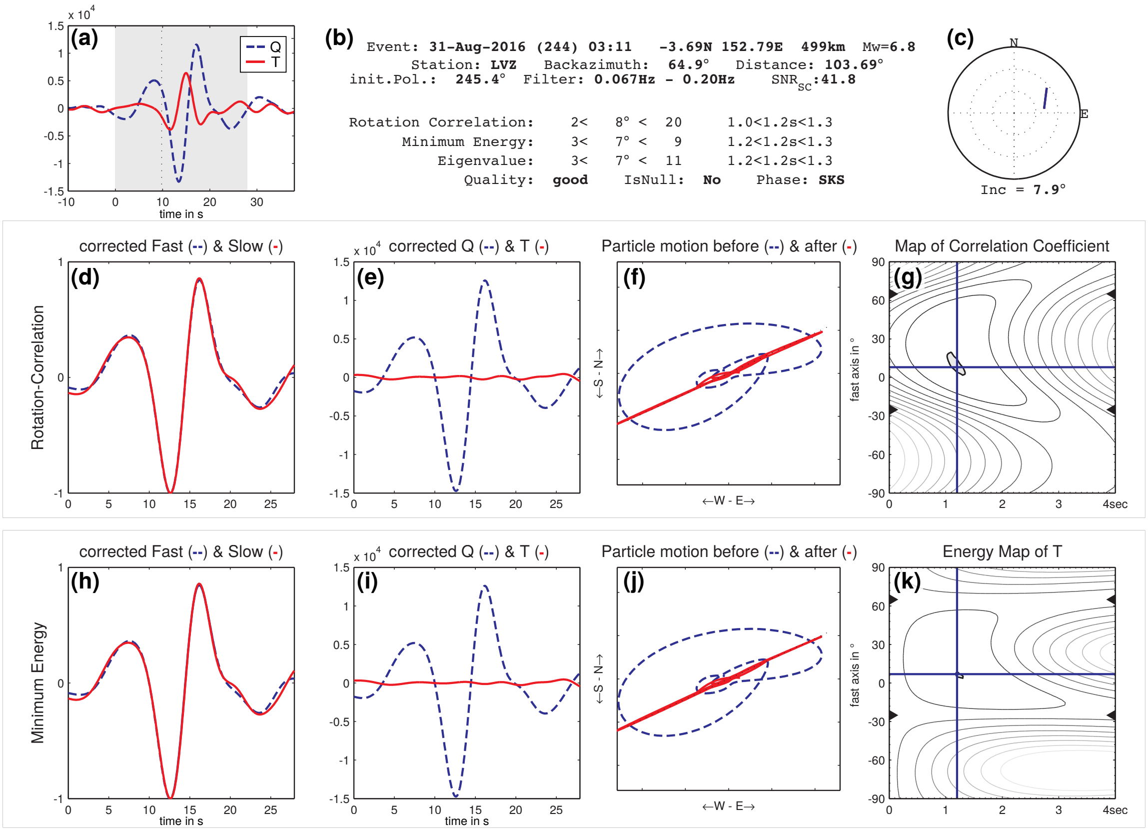

Figure 3. Diagnostic plot of a shear-wave splitting measurement with SplitLab (Wüstefeld et al., 2008) at the Russian permanent station LVZ on the Kola peninsula. (a) Original (uncorrected) radial (Q, blue dashed) and transverse (T, solid red) component seismograms. Gray area indicates the analysis window. Thin dotted line displays the theoretical arrival of the *SKS* phase based on the iasp91 Earth model (Kennett, 1991). (b) Station, event and processing information (filter, SNR, etc.) as well as splitting parameters (ϕ, δt) (with uncertainties, 95% confidence interval) resulting from the rotation-correlation method (RC, e.g. Fukao, 1984; Bowman & Ando, 1987), the energy minimization method (SC, Silver & Chan, 1991) and the eigenvalue method (EV, e.g. Silver & Chan, 1991). Quality of the measurement, null case (*yes* or *no*) and the phase name are also shown. (c) Stereoplot showing the splitting measurement as a function of backazimuth (clockwise direction from North) and incidence angle (radial axis). Results of two methods (RC and SC) are also displayed. (d)-(g) Diagnostics for the RC method showing the (d) corrected fast (blue dashed) and slow (solid red) components (normalized), (e) the corrected radial (blue dashed) and transverse (solid red) components (not normalized), (f) the initial (blue dashed) and splitting-corrected (solid red) particle motion and (g) the contour plot of the correlation coefficients with the best-fitting splitting parameters (blue lines) and the 95% confidence region (gray area). (h)-(k) Same content for the SC method. All three methods (RC, SC and EV) show nearly identical results indicating a robust measurement.

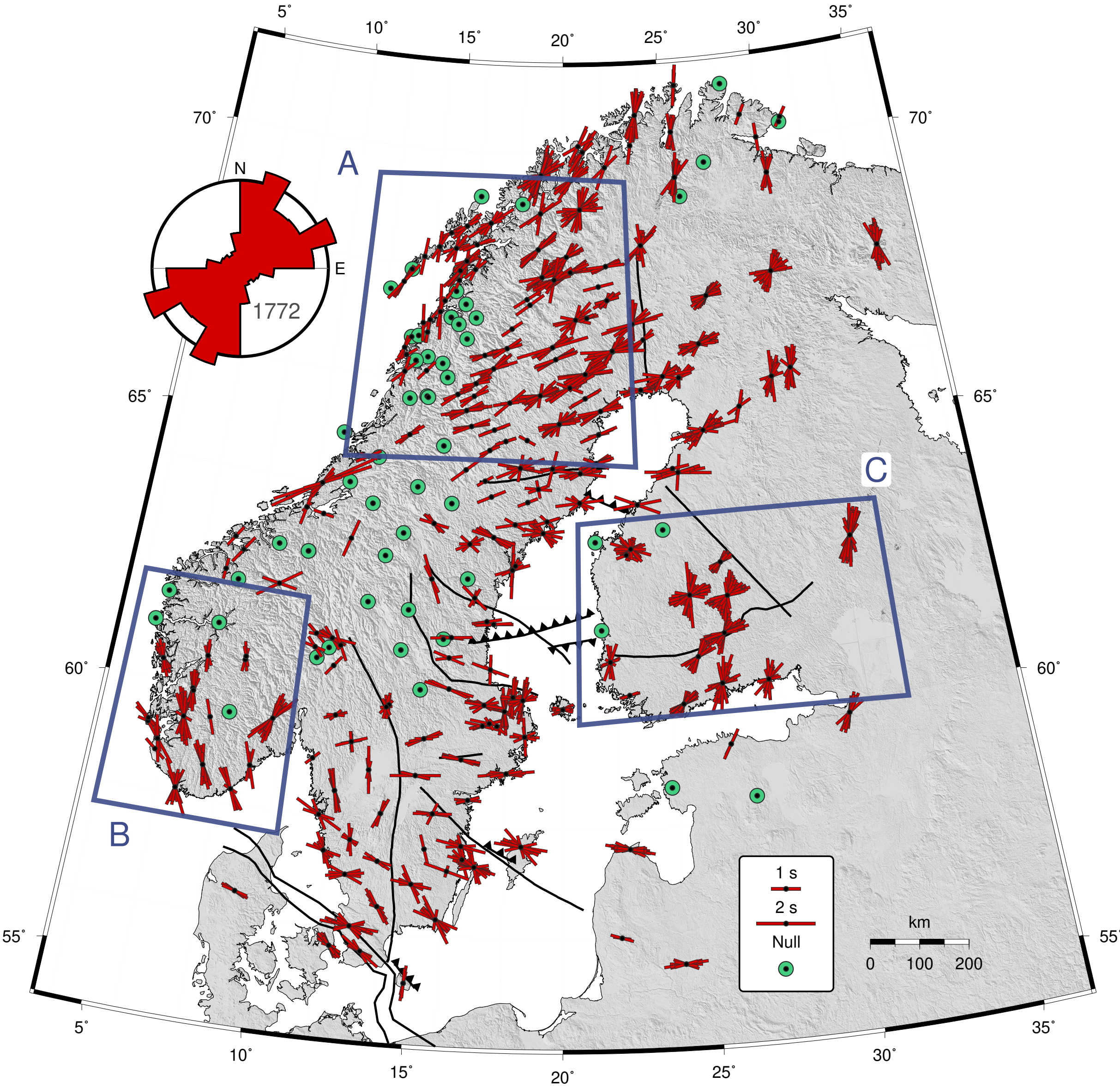

Figure 4. Summary of the 1772 individual single-phase shear-wave splitting measurements conducted at the analyzed ScanArray stations. Each split phase is represented by a red bar with the orientation indicating the fast axis ϕ relative to North and the length of each bar is scaled by the delay time δt. The overall trends for ϕ across the whole network are displayed in the rose diagram. However, in this visualization it is not possible to distinguish between different backazimuthal/incoming directions of the seismic wave (see **Figs. S10 - S15** in the Supporting Information for such a representation). Stations at which only nulls were observed are indicated by green circles. Blue boxes (A, B and C) indicate the regions for which histograms of the splitting parameters are displayed in Fig. 5.

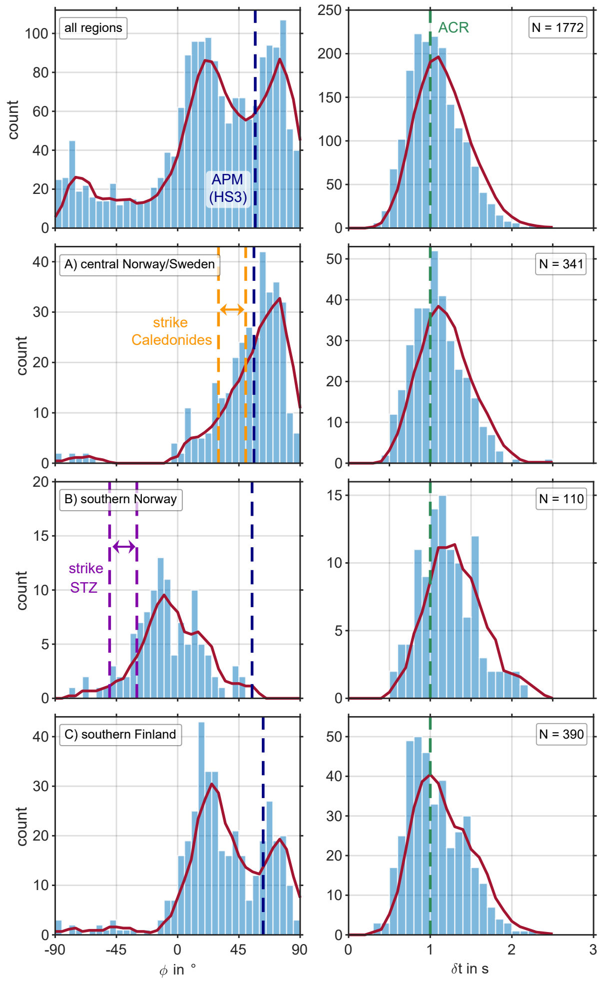

Figure 5. Histograms of the distribution of splitting parameters, separated into fast axis direction ϕ (left column panels) and delay time δt (right column panels). Top row shows distributions for the whole data set. The red curve represents a moving average of the values and highlights the trimodal distribution with peaks at around $-75°$, $22°$ and $75°$ relative to North. The average absolute plate motion directions (APM) in a hotspot reference frame (HS3) shown in the left panels (dashed blue line) were calculated with the HS3-NUVEL 1A plate motion model (Gripp & Gordon, 2002). The green dashed line in the right panels indicates the typical average value of around 1 s for continental regions (ACR, e.g. Silver, 1996; Fouch & Rondenay, 2006). The following rows display the distributions for specific areas across the study region as indicated in Fig. 4. Second row: central Norway and Sweden. The dashed orange lines indicate the range of the dominant strike direction of the Caledonian collision. Third row: southern Norway. The dashed purple lines indicate the range of the dominant strike of the Sorgenfrei-Tornquist Zone. Fourth row: southern Finland. Note the varying axis scales of the ordinates in each panel. N (upper right corners) indicates row-wise the number of values included in the histograms.

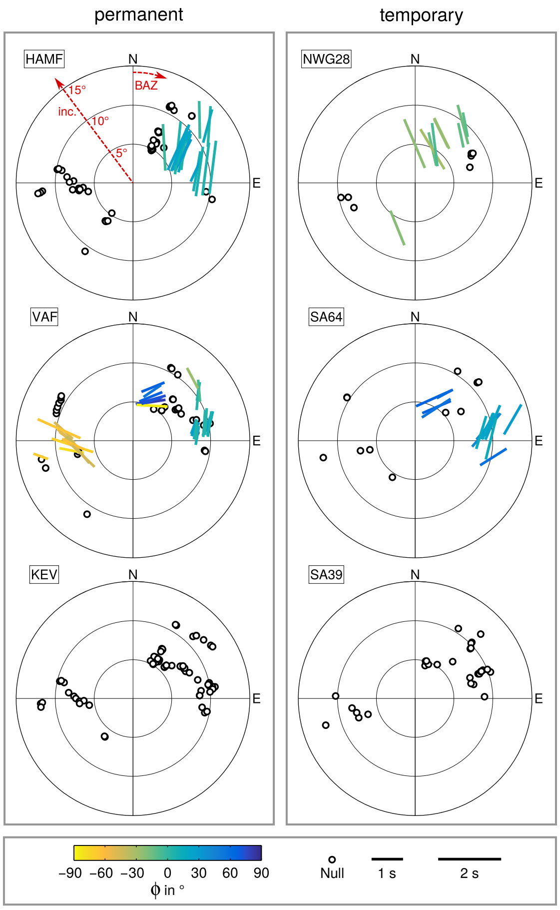

Figure 6. Exemplary stereoplots with different splitting patterns at six recording stations (for locations see Fig. 2). Splitting parameters ϕ and δt are shown as function of backazimuth (BAZ, clockwise direction from North) and incidence angle (inc., radial axis). The orientation of ϕ is additionally color-coded. Delay time δt scales with the length of the single bars. Null measurements are shown as black open circles. Left column: Observations at long-running permanent stations. Right: Splitting patterns at temporary stations with observation times of around two years. Top row: Typical examples for which the assumption of a single horizontal layer of anisotropy is valid. Although the consistent split observations (ϕ and δt) are only available for limited directions, clear nulls can be observed for the backazimuths corresponding to the fast axis direction and/or perpendicular to it. Middle row: Strong variations for the splitting parameters with backazimuth (especially for ϕ) are observed. Bottom row: Stations at which only nulls were observed for several backazimuths.

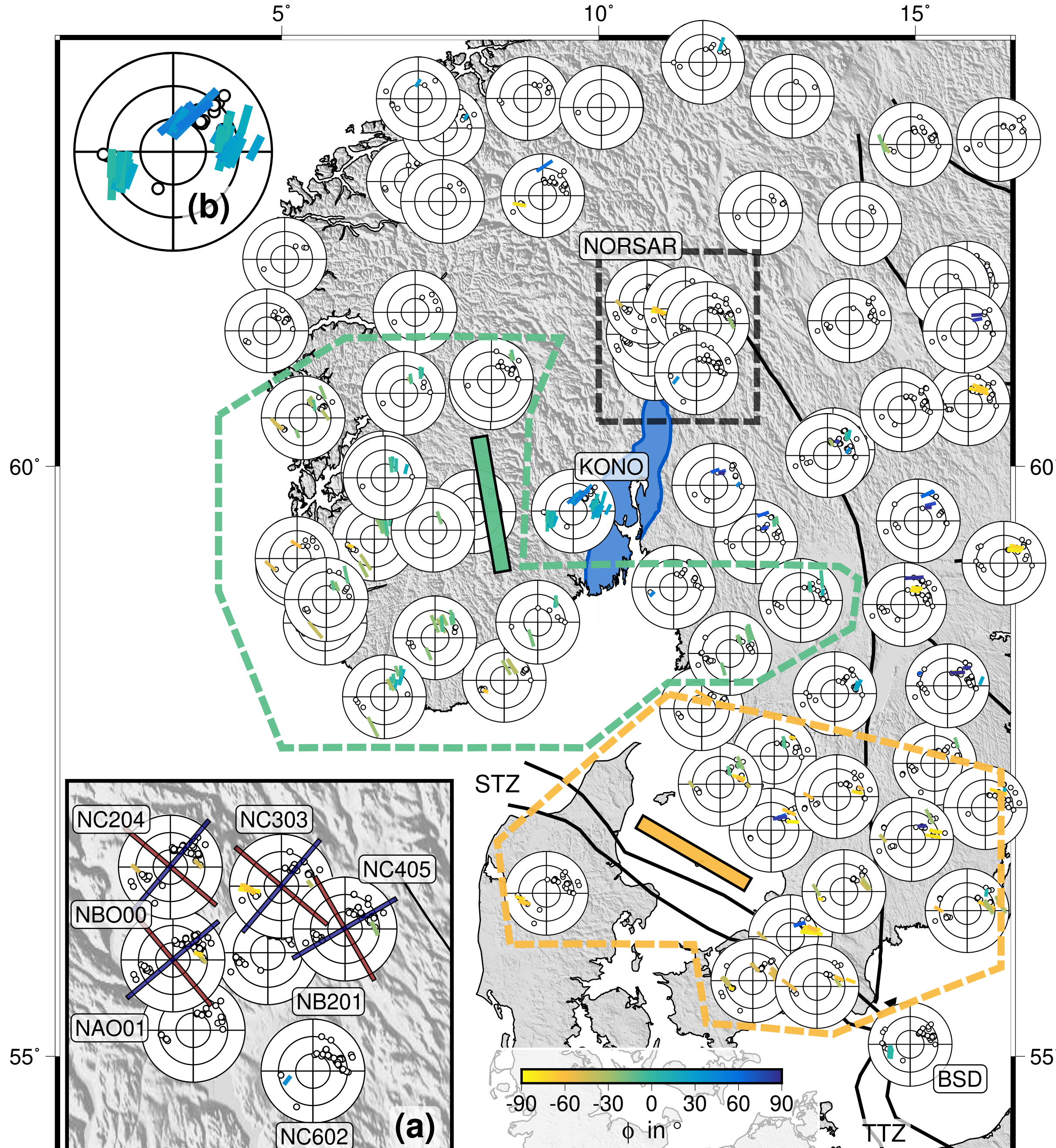

Figure 7. Distribution of stereoplots in southern Norway, Sweden and northern Denmark. The blue area indicates the Oslo Graben (OG). For plotting conventions see Fig. 6. Stations of the Norwegian Seismic Array (NORSAR, black dashed box) are shown enlarged in (a), station KONO in (b). Depending on the installation date of the instruments at NORSAR, seismic data of the period 1998-2017 were analyzed. Therefore, the patterns in general are well constrained due to the long observational period. At four stations the inferred fast and slow directions of the split waves are shown as red and blue lines, respectively.

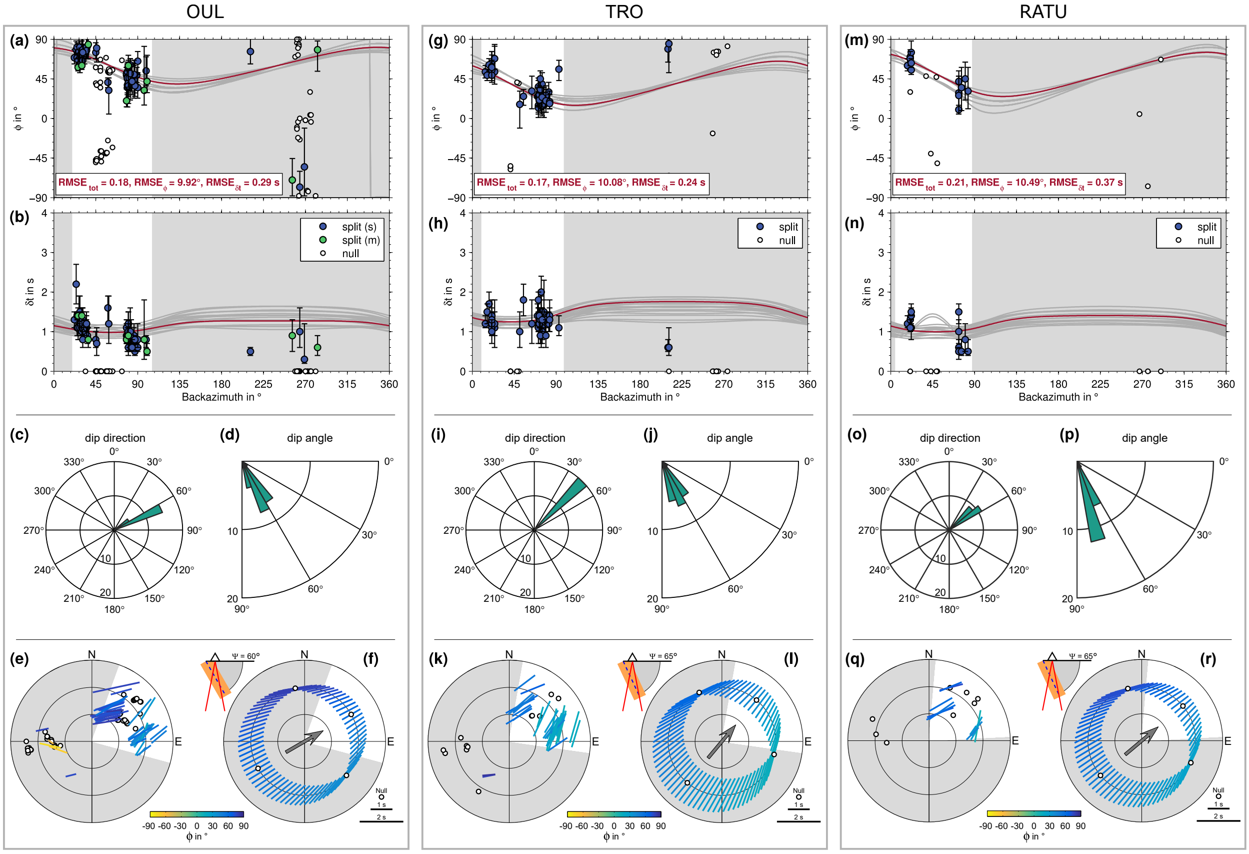

Figure 8. Exemplary modeling results for the three stations OUL, TRO and RATU (see orange circles in Fig. 2. Top row: Measured splitting parameters ϕ (a), (g), (m) and δt (b), (h), (n) plotted over backazimuth. Blue symbols with error bars (95% confidence interval) are single split measurements (only SC method shown), green ones represent multi-splits based on surface stacking using the WS method (Wolfe & Silver, 1998) as implemented in StackSplit (Grund, 2017). Small dots filled white represent null measurements. The best-fit model is highlighted as red curve and the next 19 best models are shown as gray lines. Only the measurements included in the white sector are used for the modeling. Symbols in the gray backazimuthal range are only shown for the sake of completeness. Middle row: Parameter distributions of the down-dip direction (c), (i), (o) and the layer dip (d), (j), (p) for the best models shown in the top row. Bottom row: Comparison of observed (apparent) splitting parameters (e), (k), (q) and theoretical parameters (f), (l), (r) in stereoplot view computed based on the best-fit model for a dipping symmetry axis (red curves in top row). The gray arrow shows the down-dip direction (relative to geographic North) for the synthetics. Ψ indicates the dip angle of the symmetry axis (olivine *a*-axis, dashed blue line) relative to the horizontal.

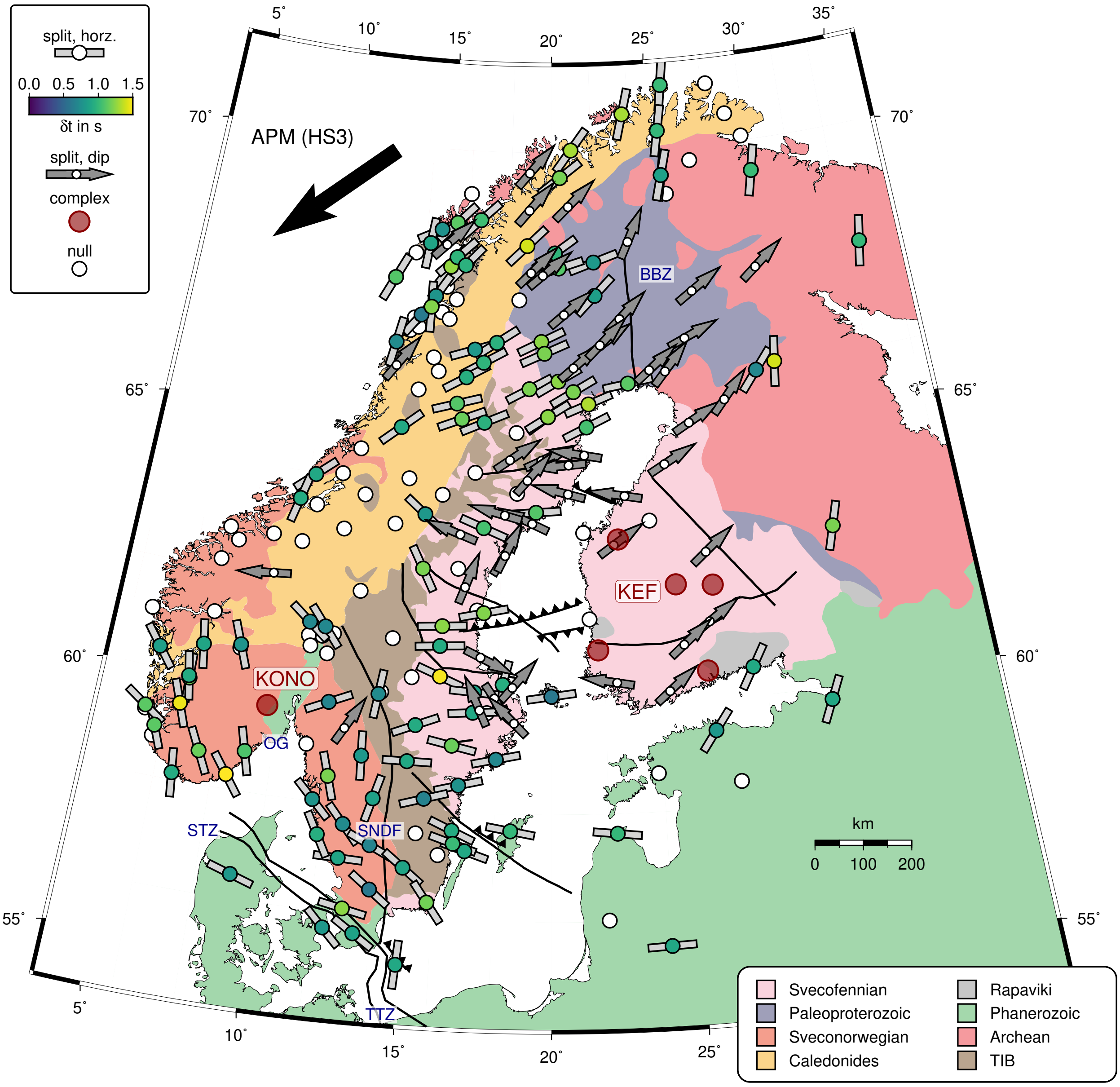

Figure 9. Map highlighting the modeling results together with the major tectonic units of Fennoscandia (background colors) after Gorbatchev (2004) and Korja & Heikkinen (2005). Stations with relatively simple splitting characteristics are shown as gray bars which indicate average values for ϕ and δt calculated with the WS method (Wolfe & Silver, 1998). The color fill of each circle represents the average delay time. Dark gray arrows indicate stations at which the data are best explained by a dipping layer of anisotropy with the arrow pointing into the down-dip direction. Stations at which the data-fit delivered non-unique models are shown as enlarged red dots (exemplary modeling for stations KONO and KEF is shown in Figs 10 and 12). Null stations are displayed as white dots with black circles. The black arrow in the upper left corner indicates the absolute plate motion direction (APM) in a hotspot reference frame (HS3-NUVEL 1A) after Gripp & Gordon (2002). For abbreviations (blue labels) see caption of Fig. 1.

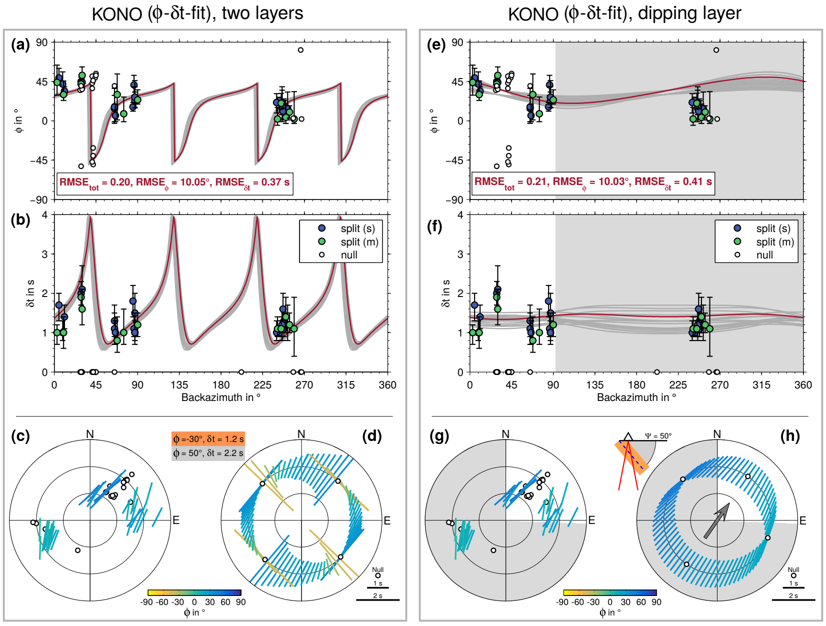

Figure 10. Two-layer and dipping-layer modeling at station KONO (see Fig. 9). Left column: Two-layer modeling based on a combined ϕ-δt-fit. Right column: Dipping layer modeling based on a combined ϕ-δt-fit for the backazimuthal range shown in white. For plotting conventions see Fig. 8.

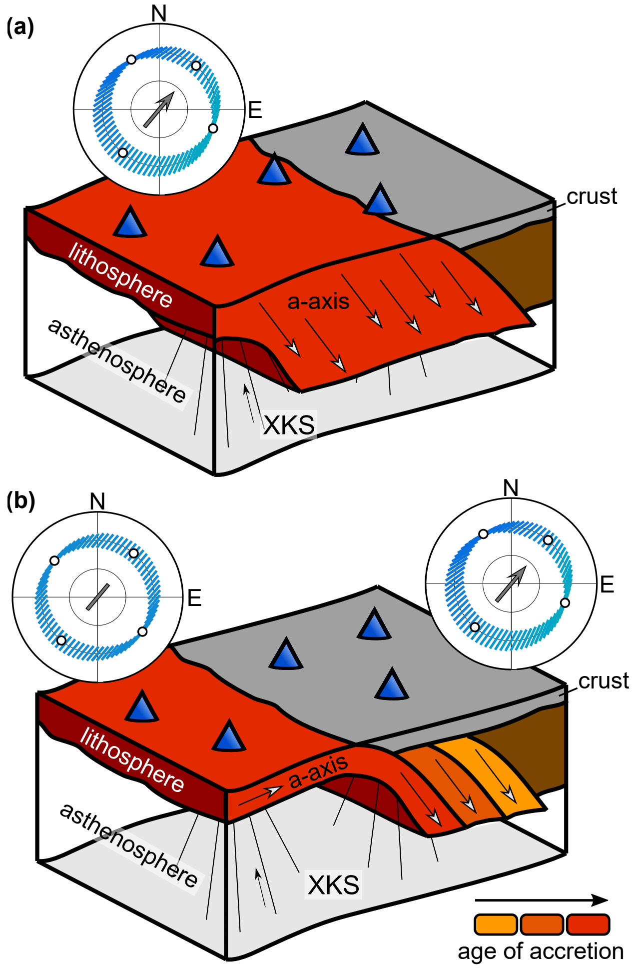

Figure 11. Schematic highlighting the most probable scenarios for the found splitting patterns in several areas of the study region. (a) The inclined fast axis direction (*a*-axis) was already imprinted into the whole lithosphere (red block) long before the formation of the Baltic Shield during the phase of craton building. (b) Several events of accretion with an existing continent lead to dipping structures with the preliminary horizontal fast axis direction inclined by a specific angle. Stations (blue triangles) on the red area registrate a splitting pattern (here synthetic) for a horizontal fast axis while the stations on the gray area see splitting due to an dipping structure. *XKS* rays (*SKS*, *SKKS*, *PKS*, *sSKS*) are shown as thin black lines.

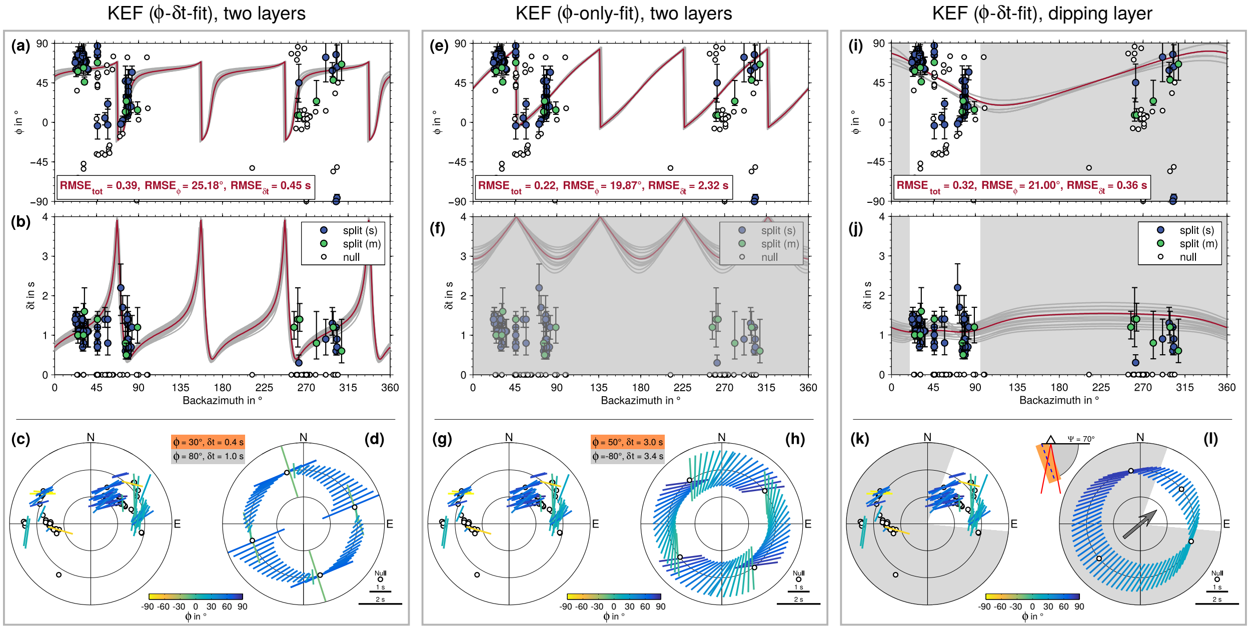

Figure 12. Exemplary two-layer and dipping-layer modeling at station KEF (see Fig. 9). First column: Two-layer modeling based on a combined ϕ-δt-fit. For plotting conventions see Fig. 8. Middle column: Two-layer modeling based on a ϕ-only-fit. The total RMSE displayed in (e) is only calculated from the ϕ-fit. Bar lengths in (h) are uniformly scaled to 2 s and do not represent the true delay times δt of the corresponding best-fit models (f) since they would extend over the radial axis limits. Right column: Dipping layer modeling based on a combined ϕ-δt-fit for the backazimuthal range shown in white.

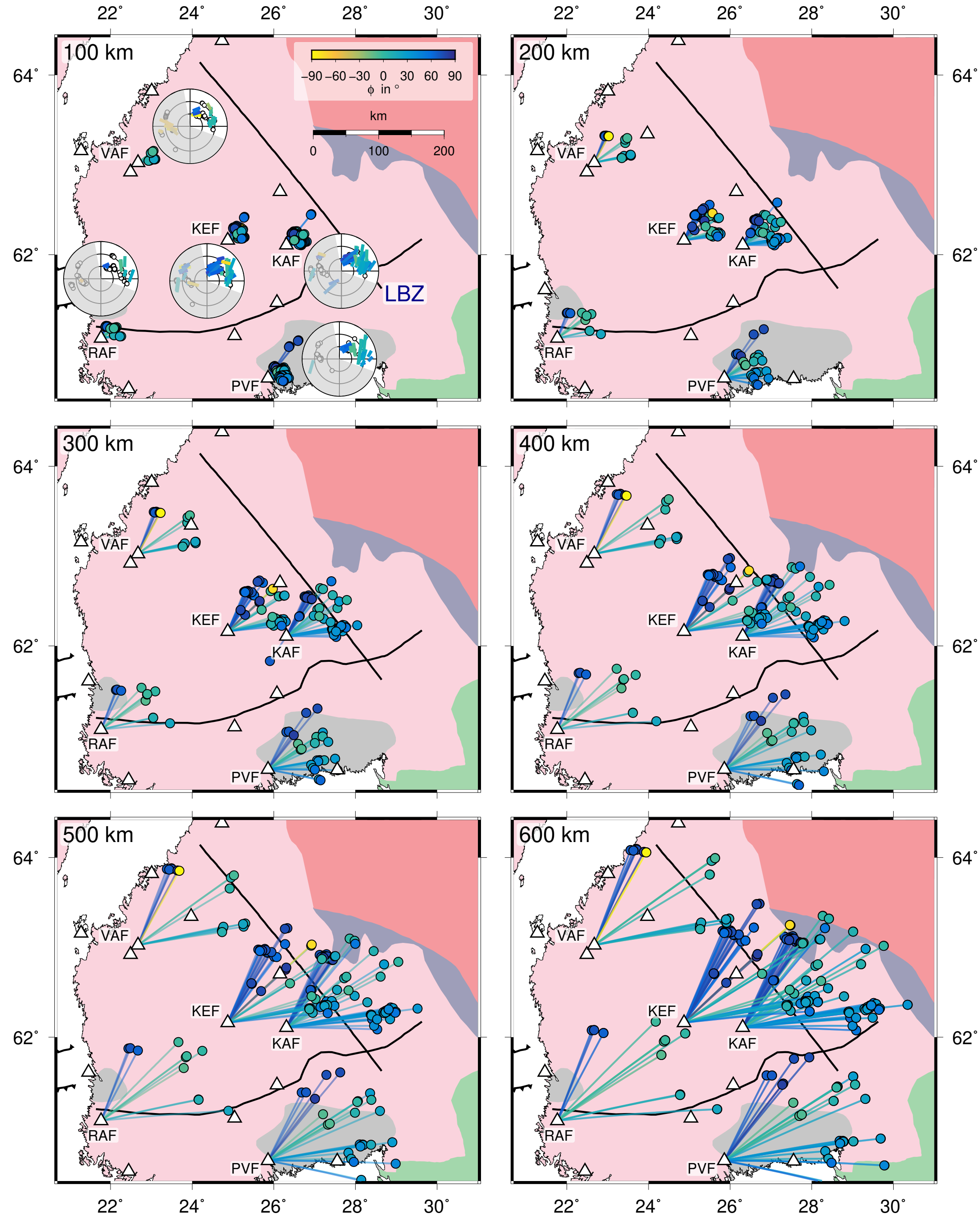

Figure 13. Pierce points (circles) in different depth ranges (100 km-600 km) and raypaths (lines) from the corresponding depth to the recording station at the surface (triangles). Pierce points and raypaths are color-coded with respect to the observed fast axis direction (see stereoplots of the five stations in the upper left panel). Raypaths and pierce points are only shown for events from northeast (white sector). For geological units see Fig. 1.

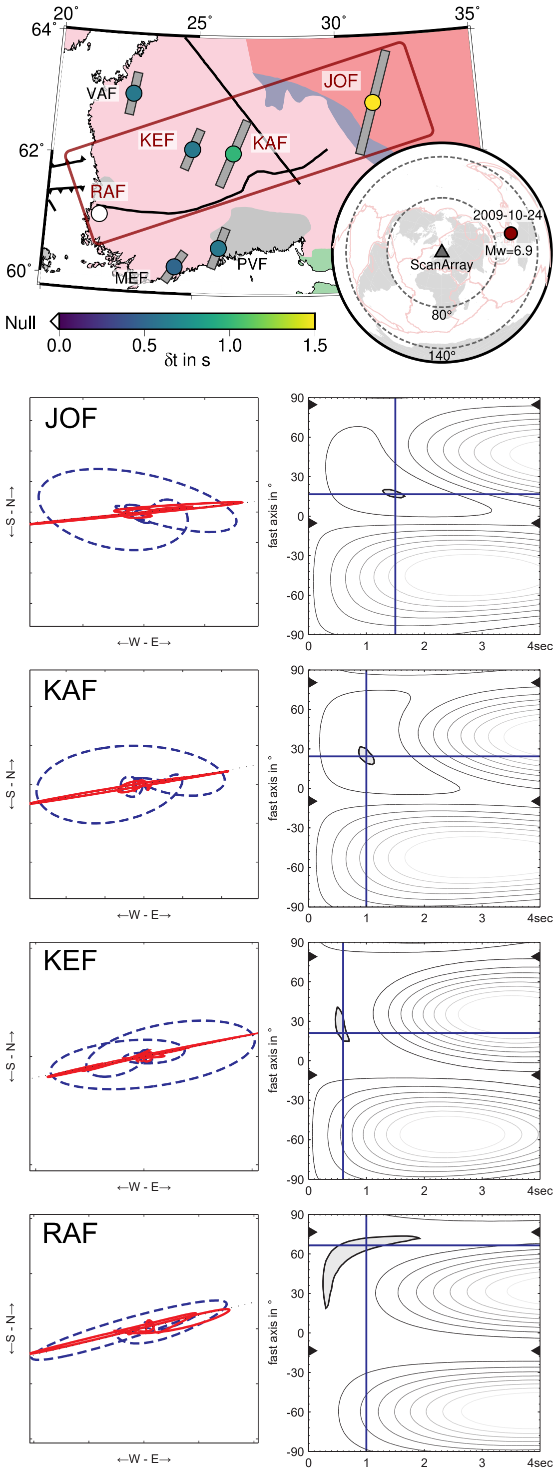

Figure 14. Particle motion plots (left column) and minimum energy surfaces (right) for the *SKS* phase of one earthquake (2009-10-24) recorded at four stations (JOF, KAF, KEF, RAF) located roughly along a line in southern Finland (top panel, red box). Stations PVF, MEF and VAF are shown for the sake of completeness. Delay times δt decrease from east to west while the fast axis orientation ϕ is almost in the same direction at all stations. At RAF the almost linear particle motion as well as the elongated 95% confidence area (dark gray) indicate a near-null case (e.g. Wüstefeld & Bokelmann, 2007). For geological units see Fig. 1.

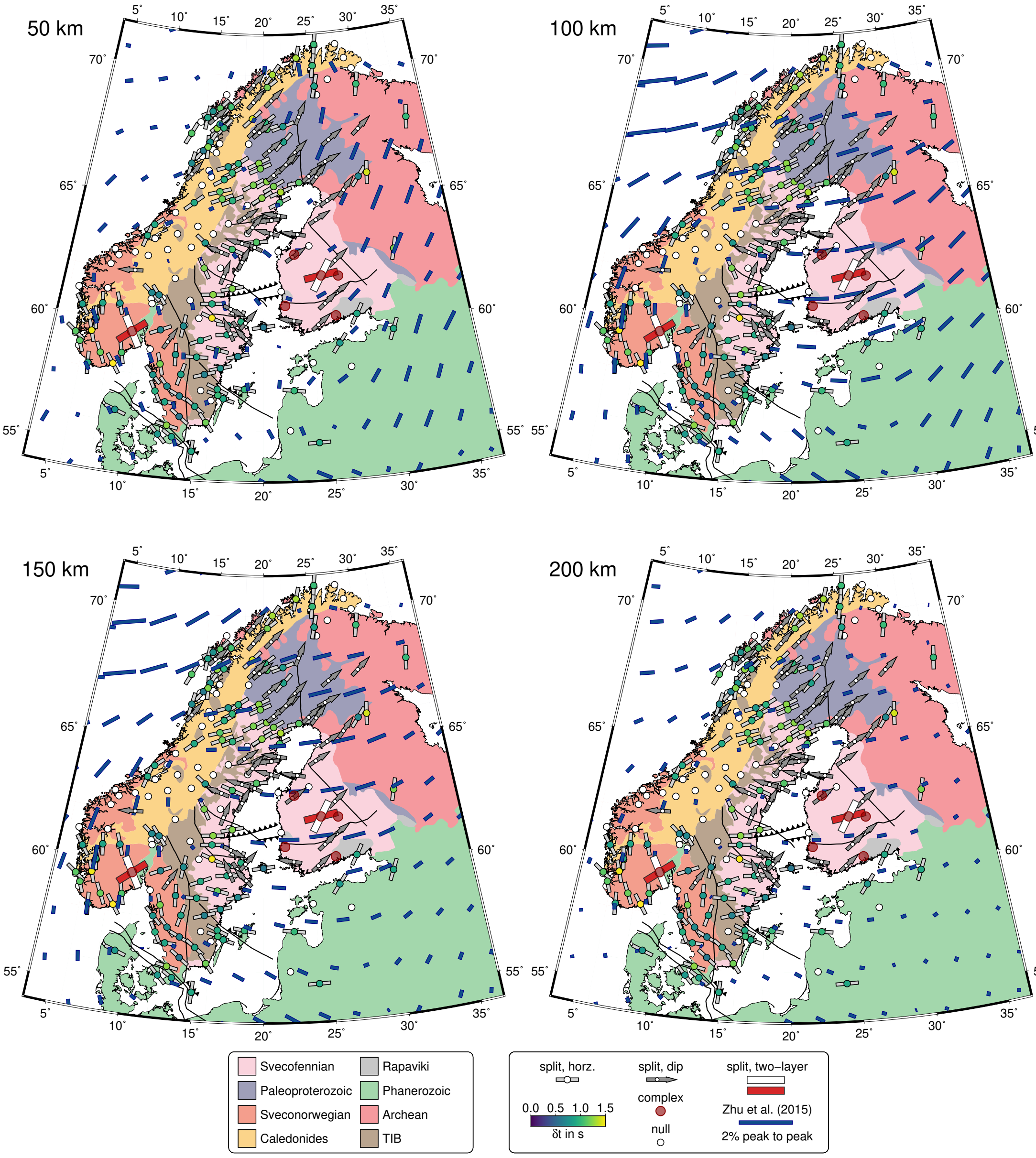

Figure 15. Shear-wave splitting modeling results and major tectonic units as in Fig. 9 together with the estimates of azimuthal anisotropy derived from surface-wave tomography (Zhu & Tromp, 2013; Zhu et al., 2015) in different depths (50 km, 100 km, 150 km, and 200 km). The directions and amplitudes of the fast axes from surface-wave tomography are given by the orientations and lengths of the blue bars. Orientations of ϕ for possible two-layer scenarios at stations KONO and KEF are displayed as white (upper layer) and red (lower layer) bars.

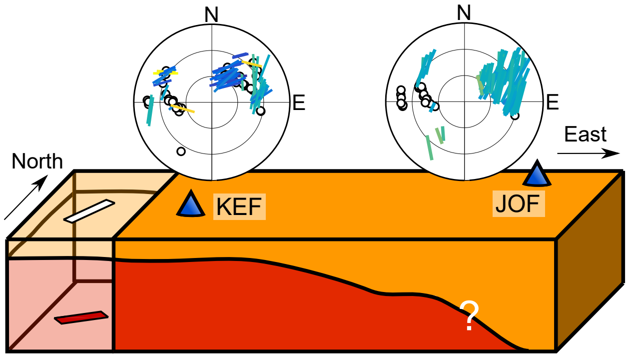

Figure 16. Schematic displaying a possible scenario for southern Finland. The model consists of two anisotropic layers in the west with an increase in thickness of the upper layer to the east. This is supported by the complex splitting pattern observed at recording station KEF, the simple characteristics at station JOF as well as the observations highlighted in Fig. 14. Please note, dimensions of the sketch are not drawn to scale.